Tellurapyrylium dyes. 2. The electron-donating properties of the chalcogen atoms to the chalcogenapyrylium nuclei and their radical dications, neutral radicals, and anions

Michael R. Detty, J. M. McKelvey, and H. R. Luss

Organometallics, **1988**, 7 (5), 1131-1147• DOI: 10.1021/om00095a019 • Publication Date (Web): 01 May 2002

dependence on sin θ. The final agreement factors were $R = 0.056$ and $R_w = 0.078$.

Acknowledgment. We gratefully acknowledge the financial support of the National Science Foundation (CHE 84-20768) in support of this work.

Registry No. *trans*-$(NBu_4)[OS(N)(CH_2SiMe_3)_2Cl_2]$, 92544-01-9; *cis*-$[NBu_4][Os(N)(CH_2SiMe_3)_2(SCH_2CH_2)]$, 113109-68-5; *cis*-$[NBu_4][Os(N)(CH_2SiMe_3)_2(SCN)_2]$, 113109-72-1; *cis*-$[NBu_4][Os(N)(CH_2SiMe_3)_2(SCN)(NCS)]$, 113109-70-9; *cis*-$[Os(N)(CH_2SiMe_3)_2(SNC_5H_4)]_2$, 113132-20-0; *trans*-$[Os(N)(CH_2SiMe_3)_2(SNC_5H_4)]_2$, 113215-75-1; ethanedithiol, 540-63-6; 2-pyridinethiol, 2637-34-5.

Supplementary Material Available: Tables of hydrogen positional parameters, thermal parameters, distances and angles, and planes (5 pages); a listing of final observed and calculated structure factor amplitudes (21 pages). Ordering information is given on any current masthead page.

Tellurapyrylium Dyes. 2. The Electron-Donating Properties of the Chalcogen Atoms to the Chalcogenapyrylium Nuclei and Their Radical Dications, Neutral Radicals, and Anions

M. R. Detty,* J. M. McKelvey,* and H. R. Luss

Corporate Research Laboratories, Eastman Kodak Company, Rochester, New York 14650

Received September 30, 1987

Several series of chalcogenapyrylium dyes were prepared and were examined by absorption spectroscopy and cyclic voltammetry. Substitution of the heavier chalcogens for oxygen in each series gave sequential bathochromic shifts in the absorption maxima in the order O < S < Se < Te, gave less positive oxidation potentials in the order O < S < Se < Te, and gave less negative reduction potentials in the order O < S < Se < Te (with the pyrylium nucleus having the most negative reduction potential and the tellurapyrylium nucleus, the least negative). The redox data suggest that π-donation from the heteroatom to the carbon π-framework is important in determining the stability of the various states. The chalcogenapyranyl radicals can be oxidized to the Hückel aromatic chalcogenapyranyl anion. The oxidation of the radicals is increasingly positive in the order O < S < Se < Te while reduction of the radicals is increasingly negative in the order Te < Se < S < O. The decreased aromaticity and antiaromaticity as the size of the chalcogen increases would be expected with the larger available orbitals leading to less effective π-bonding. The structure of **6d**, as determined by single-crystal X-ray crystallography, also illustrates the differences in π-bonding between the pyrylium nucleus and the tellurapyrylium nucleus. The molecule, 4-[2,6-diphenyl-4*H*-pyran-4-ylidene)methyl]-2,6-diphenyltellurapyrylium fluoroborate, crystallizes in monoclinic space group 2_1C with $Z = 4$, $a = 13.877$ (2) Å, $b = 11.344$ (4) Å, $c = 19.600$ (2) Å, and $\beta = 106.654$ (11)°. In **6d**, single bonds are shorter and double bonds are longer in the pyrylium ring relative to the tellurapyrylium ring. MNDO calculations were performed on model pyrylium and thiapyrylium systems. Ionization potentials from the calculations as predicted by Koopmans' theorem do not track the experiment oxidation potentials as determined by cyclic voltammetry; theory predicts raising the magnitude of oxidation via a lowering of the HOMO energy level upon substitution of sulfur for oxygen. Both theory and experiment agree on the influence of the heteroatom with respect to electron affinities and reduction potentials. In each case, substitution of sulfur for oxygen is predicted to lower the LUMO energy level. The use of ΔSCF values for heats of formation of the completely optimized species involved (the parent chalcogenapyrylium nucleus, the radical dication, the neutral radical, and the anion) as determined by MNDO and/or AM1 calculations for the pyrylium and thiapyrylium species do track the trends observed in values of $E^{\circ\prime}$ by cyclic voltammetry. This suggests that values of $E^{\circ\prime}$ for oxidation and reduction parallel the adiabatic gas-phase ionization potentials and electron affinities, respectively. MNDO determined HOMO – LUMO gaps for model pyrylium and thiapyrylium dyes give a linear correlation with the energies of the experimental absorption maxima for 2,6-diphenyl- and 2,6-di-*tert*-butyl-substituted pyrylium and thiapyrylium derivatives. The magnitude of the heteroatom effect on oxidation and reduction potentials can be predicted by the magnitude of the coefficients at the heteroatom positions in the HOMO and LUMO of the model systems.

Introduction

The relative σ- and π-electron-donating behavior of chalcogens (oxygen, sulfur, selenium, and tellurium) and the heteroatom effect on stabilizing adjacent carbon ion and carbon radical centers have been areas of interest.[1-5] In particular, the chalcogen atom effect on the oxidation potentials of neutral chalcogen-containing donors such as the tetrachalcogenafulvalenes,[2] 5,6:11,12-bis(dichalcogeno)tetracenes,[3] and the (chalcogenapyranyl)-chalcogenapyrans[4] have been well-studied. In cyclic

(1) (a) Saeva, F. D.; Olin, G. R. *J. Am. Chem. Soc.* **1980**, *102*, 299. (b) Boutique, J. P.; Verbist, J. J.; Fripiat, J. G.; Delhalle, J. *J. Chem. Soc., Perkin Trans. 2* **1984**, 240. (c) Pau, J. K.; Ruggera, M. B.; Kim, J. K.; Caserio, M. C. *Ibid.* **1978**, *100*, 4242 and references cited therein.

(2) (a) Wudl, F.; Aharon-Shalom, *J. Am. Chem. Soc.* **1982**, *104*, 1154. (b) Lerstrup, K.; Talham, D.; Bloch, A.; Poehler, T.; Cowan, D. *J. Chem. Soc., Chem. Commun.* **1982**, 336. (c) McCullough, R. D.; Kok, G. B.; Lerstrup, K. A.; Cowan, D. O. *J. Am. Chem. Soc.* **1987**, *109*, 4115.

(3) Jones, M. T.; Jansen, S.; Acampora, L. A.; Sandman, D. J. *J. Phys. (Les Ulis, Fr.)* **1983**, *44*, C3-1159.

(4) (a) Perlstein, J. H. *Angew. Chem., (Les Ulis, Fr.) Int. Ed. Engl.* **1977**, *16*, 519. (b) Perlstein, J. H.; Van Allan, J. A.; Isett, L. C.; Reynolds, G. A. *Ann. N. Y. Acad. Sci.* **1978**, *313*, 61. (c) Detty, M. R.; Hassett, J. W.; Murray, B. J.; Reynolds, G. A. *Tetrahedron* **1985**, *41*, 4853. (d) Sandman, D. J.; Holmes, T. J.; Warner, D. E. *J. Org. Chem.* **1979**, *44*, 880. (e) Chasseau, D.; Gaultier, J.; Hauw, C.; Fugnitto, R.; Gionis, V.; Strzelecka, H. *Acta Crystallogr., Sect. B: Struct. Crystallogr. Cryst. Chem.* **1980**, *B38*, 1629.

(5) Bock, H.; Brahler, G.; Dauplaise, D.; Meinwald, J. *Chem. Ber.* **1981**, *114*, 2622.

0276-7333/88/2307-1131$01.50/0

Scheme I

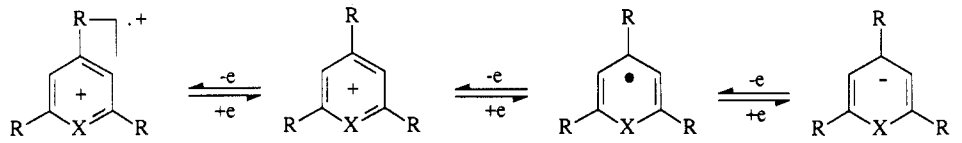

1, X = O, S, Se, Te

voltammograms of these systems, the first oxidation becomes increasingly positive as the chalcogens become larger. In the naphthalene-1,8-dichalcogenides, the chalcogen atom exerts little influence on the first ionization potential as determined by photoelectron spectroscopy.[5]

The relative electron-donating abilities of oxygen and sulfur have been studied by Saeva and Olin[1a] in the cationic pyrylium and thiapyrylium ring systems. The redox potentials of two pairs of pyrylium and thiapyrylium salts were correlated with the spectral properties of the same systems.[1a] Such studies have not been extended to include selena- and tellurapyrylium dyes which have only recently been prepared.[6]

The chalcogenapyrylium nuclei **1** form discrete cation/dication, cation/radical, and radical/anion redox couples, as shown in Scheme I,[1a] which makes these systems ideal for comparing the effects of the chalcogen atoms on adjacent ionic and radical centers. These effects would be easily measured by changes in the redox potentials of the systems. The chalcogens become more electropositive as size increases which suggests that oxidation of a system should become less possitive as the chalcogen size increases based on σ-donor properties. However, as the chalcogens increase in size, overlap of the heteroatom orbitals with the carbon π-framework would become less efficient and would be expected to affect the π-donating ability of the heteroatom. The σ- and π-electron-donating abilities of the chalcogens have been studied by theoretical methods in many of the systems described above. In an ab initio comparison of pyranylpyran with thiapyranylthiapyran, the highest occupied molecular orbital (HOMO) of the thiapyranylthiapyran was found to lie 0.21 eV higher in energy than in the pyranylpyran.[1b] In these two systems, changing the heteroatoms influenced the planarity of the system as well as carbon–carbon bond lengths. A Hückel MO study of the naphthalene-1,8-dichalcogenides showed little effect of the chalcogen atoms on the eigenvalues of the HOMO's in these systems.[5] CNDO[7] and Hückel MO[8] studies of the pyrylium ring have shown that the π-orbitals are benzene-like. Hückel MO studies of the thiapyrylium nucleus predict no change in the eigenvalue of the HOMO relative to the pyrylium nucleus and a lowering of the eigenvalue of the lowest unoccupied molecular orbital (LUMO) by 0.4 eV relative to the pyrylium nucleus.[8] All computations on these systems that have been reported to date have been on the closed-shell systems.

We report our study of the chalcogenapyrylium nuclei which has both a computational and an experimental component. We report using the MNDO procedure[9] [which is generally calibrated to give geometries, ionization potentials (IP's), heats of formation (H_f), and dipole moments] to examine the pyrylium and thiapyrylium nuclei. Furthermore, we are reporting for the first time results for a restricted Hartree–Fock MNDO procedure that was efficiently performed on open-shell systems. We can now evaluate geometry distortions relative to the closed-shell systems for the addition and removal of electrons for the pure spin state. This also allows, for the first time, computation of ΔSCF IP's for the MNDO method[9] which can be compared with Koopmans' theorem values (eq 1 and 2).[10]

$$IP = -\epsilon_{HOMO} \quad (1)$$

$$EA = \epsilon_{LUMO} \quad (2)$$

A quantitative evaluation of the ability of oxygen, sulfur, selenium, and tellurium atoms to stabilize adjacent radical and ionic centers and to alter absorption spectra and related phenomena within a common carbon skeleton should be possible. We have investigated several series of chalcogenapyrylium dyes including selenapyrylium and tellurapyrylium salts in addition to the pyrylium and thiapyrylium analogues by cyclic voltammetry (CV) and absorption spectroscopy. These studies allow the contributions of the chalcogenapyrylium nuclei, and the chalcogen atoms themselves, to the stability of radical and ionic centers and to differences in absorption spectra to be separated and evaluated. In particular, selena- and tellurapyrylium dyes have been examined for the first time in this context.

The donor and acceptor properties of dye molecules as well as their electronic excitations are linked to the energy of highest occupied (HOMO) and lowest unoccupied (LUMO) molecular orbitals. Experimental information about these orbitals can be gained from both CV and spectroscopic techniques. The CV time scale is much slower[11] than the time scale for the absorption of a photon.[12] While the CV process allows equilibrium conditions to be observed for both oxidation and reduction, the absorption of a photon involves a nonadiabatic promotion of an electron. The differences in time scale might become important in comparisons of oxidation and reduction potentials with the energy of the absorption of a photon.

Experimental Results

Preparation of Materials. The chalcogenapyrylium dyes **2** through **10** and other dyes described in this study were prepared by literature procedures or extensions of literature procedures.[6] The synthetic techniques are summarized in Scheme II. The physical and spectral properties of these dyes are compiled in Table I.

Several different counter ions were employed in this study. The choice of counterion was often dictated by the availability of starting materials. The hexafluoro-

(6) (a) Detty, M. R.; Murray, B. J. *J. Org. Chem.* **1982**, *47*, 5235. (b) Detty, M. R.; Luss, H. R. *Organometallics* **1986**, *5*, 2250.
(7) Bigelow, R. W. *J. Chem. Phys.* **1977**, *67*, 4498.
(8) Pragst, F.; Janda, M.; Stibor, I. *Electrochim. Acta* **1980**, *25*, 779.
(9) (a) Dewar, M. J. S.; Thiel, W. *J. Am. Chem. Soc.* **1977**, *99*, 4899. (b) Dewar, M. J. S.; Thiel, W. *Ibid.* **1977**, *99*, 4907.
(10) (a) Koopmans, T. *physica* **1933**, *1*, 1453. (b) Michl, J.; Thulstrup, E. W. *Tetrahedron* **1976**, *32*, 205.
(11) Bard, A. J.; Faulkner, L. R. *Electrochemical Methods*; Wiley: New York, 1980.
(12) Turro, N. J. *Modern Molecular Photochemistry*; Benjamin Cummings: Menlo Park, CA, 1978.

Table I. Physical and Spectral Properties of Chalcogenapyrylium Dyes 2–10

compd	X	Y	Z	mp, °C	solv	λ_{max} (log ϵ), nm	$E_{\lambda_{max}}$, eV
2a	Te		BF_4	195–197	CH_3CN	591 (4.84)	2.10
					CH_2Cl_2	610 (4.81)	2.03
2b	Se		ClO_4	241–242	CH_3CN	555 (4.81)	2.23
2c	S		ClO_4	266–267	CH_3CN	524 (4.80)	2.37
					CH_2Cl_2	543 (4.79)	2.29
2d	O		BF_4	277–281	CH_3CN	487 (4.75)	2.54
					CH_2Cl_2	495 (4.76)	2.51
3a	Te		BF_4	178–179	CH_3CN	758 (5.15)	1.64
					CH_2Cl_2	775 (5.16)	1.60
3b	Se		BF_4	193–195	CH_3CN	717 (5.12)	1.73
3c	S		BF_4	211.5–213	CH_3CN	660 (5.10)	1.88
					CH_2Cl_2	698 (5.14)	1.77
3d	O		ClO_4	206.5–207	CH_3CN	637 (5.11)	1.95
4a	Te	Te	BF_4	239–240	CH_3CN	695 (5.11)	1.79
					CH_2Cl_2	715 (5.11)	1.74
4b	Te	Se	BF_4	223–227	CH_3CN	655 (4.99)	1.90
					CH_2Cl_2	674 (4.98)	1.84
4c	Te	S	BF_4	215–218	CH_3CN	632 (5.00)	1.96
					CH_2Cl_2	651 (5.01)	1.91
4d	Te	O	BF_4	241–243	CH_3CN	576 (5.01)	2.16
					CH_2Cl_2	594 (5.00)	2.09
4e	Se	Se	ClO_4	253–254	CH_3CN	605 (5.15)	2.05
					CH_2Cl_2	623 (5.15)	1.99
4f	Se	S	ClO_4	245 dec	CH_2Cl_2	599 (5.01)	2.07
4g	Se	O	ClO_4	241–243	CH_2Cl_2	549 (5.02)	2.26
5a	Te		BF_4	200–202	CH_3CN	636 (4.76)	1.95
					CH_2Cl_2	653 (4.83)	1.90
5b	Se		BF_4	211–213	CH_3CN	603 (4.80)	2.06
					CH_2Cl_2	620 (4.81)	2.00
5c	S		BF_4	235–238	CH_3CN	583 (4.82)	2.13
					CH_2Cl_2	592 (4.83)	2.10
5d	O		BF_4	256–257	CH_3CN	542 (4.89)	2.29
					CH_2Cl_2	550 (4.91)	2.26
6a	Te	Te	BF_4	225–227	CH_3CN	749 (5.20)	1.66
					CH_2Cl_2	759 (5.20)	1.64
6b	Te	Se	BF_4	208–209	CH_3CN	703 (5.11)	1.77
					CH_2Cl_2	722 (5.00)	1.72
6c	Te	S	BF_4	213–215	CH_3CN	706 (5.10)	1.76
					CH_2Cl_2	690 (5.11)	1.80
6d	Te	O	BF_4	269–271	CH_3CN	645 (5.04)	1.92
					CH_2Cl_2	650 (5.14)	1.91
7a	Te	Te	PF_6	149–155	CH_2Cl_2	834 (4.85)	1.49
7b	Te	Se	PF_6	151–156	CH_2Cl_2	795 (4.85)	1.56
7c	Te	S	PF_6	161–166	CH_2Cl_2	762 (4.74)	1.63
7d	Te	O	PF_6	171–177	CH_2Cl_2	720 (4.75)	1.72
7e	Se	Se	PF_6	193–195	CH_2Cl_2	746 (4.93)	1.66
7f	Se	S	PF_6	151–158	CH_2Cl_2	721 (4.69)	1.72
7g	Se	O	PF_6	228–231	CH_2Cl_2	678 (4.82)	1.83
8a	Te	Te	BF_4	205–208	CH_2Cl_2	828 (5.52)	1.50
8b	Te	Se	BF_4	199–202	CH_2Cl_2	786 (5.45)	1.58
9a	Te	Te	BF_4	200–202	CH_2Cl_2	843 (5.42)	1.47
9b	Te	Se	ClO_4	191–195	CH_2Cl_2	803 (5.44)	1.55
10a	Te	Te	BF_4	280–282	CH_2Cl_2	885 (5.45)	1.40
10b	Te	Se	ClO_4	241–244	CH_2Cl_2	843 (5.26)	1.47
10c	Te	S	ClO_4	245 dec	CH_2Cl_2	820 (5.30)	1.51
10d	Te	O	BF_4	251–252	CH_2Cl_2	780 (5.35)	1.59

phosphate, tetrafluoroborate, and perchlorate salts of **2a**, **2c**, **4a**, **5a**, and **6a** were all examined spectroscopically. Within experimental error (±2 nm for λ_{max}, 5% for ϵ), the counterion made no difference in the absorption spectra of the dyes in this study in the concentration ranges examined (10^{-4}–10^{-5} M). Similarly, the counterion had no effect on the cyclic voltammograms of these same dyes at 5×10^{-4} M concentration with tetra-*n*-butylammonium fluoroborate as supporting electrolyte.

Compounds **2–10** embody a variety of structural features. The chalcogens have been incorporated into common carbon frameworks allowing the systematic comparison of the effects of the chalcogenapyrylium nuclei and the chalcogens on ion and radical stability. The phenyl and *tert*-butyl substituents at the 2- and 6-positions allow the contrast of substituents that are either incapable or capable of conjugative interaction with the chalcogenapyrylium ring. The steric and electronic effects of the methyl substituents in the methine backbones of **7** and **9** can be compared with the unsubstituted analogues **6** and **8**, respectively.

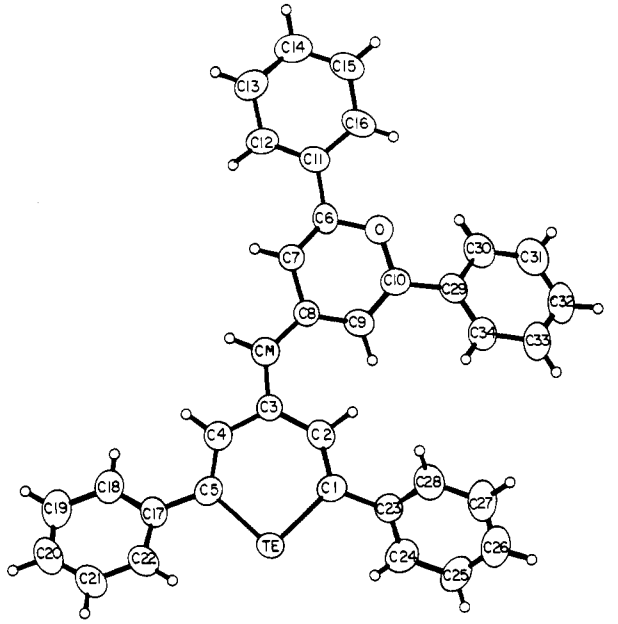

Figure 1. Plot of **6d** with BF_4 anion omitted for clarity.

Table II. Selected Bond Distances (Å) and Angles (deg) in 6d

atom 1	atom 2	dist[a]	atom 1	atom 2	atom 3	angle[a]
Te	C1	2.067 (5)	C1	Te	C5	94.3 (2)
Te	C5	2.069 (5)	Te	C1	C2	122.0 (3)
C1	C2	1.358 (6)	Te	C5	C4	121.6 (3)
C2	C3	1.441 (6)	C1	C2	C3	129.3 (4)
C3	C4	1.434 (6)	C2	C3	C4	122.3 (4)
C4	C5	1.370 (6)	C3	C4	C5	129.4 (4)
O	C6	1.378 (5)	C6	O	C10	119.7 (4)
O	C10	1.359 (5)	O	C6	C7	120.1 (4)
C6	C7	1.340 (6)	O	C10	C9	121.0 (4)
C7	C8	1.416 (6)	C6	C7	C8	122.8 (4)
C8	C9	1.428 (6)	C7	C8	C9	114.3 (4)
C9	C10	1.348 (6)	C8	C9	C10	121.6 (4)

[a] Numbers in parentheses are estimated standard deviations in the least significant digits.

X-ray Crystal Structure of 6d. The size of the chalcogens increases from a covalent radius of 0.73 Å for oxygen to 1.36 Å for tellurium. One would expect the substitution of the larger chalcogens for oxygen in the chalcogenapyrylium ring to alter the geometry of the ring. Monomethine dye **6d** illustrates the two extremes in the chalcogenapyrylium dye series with a pyrylium nucleus in one ring and a tellurapyrylium nucleus in the other. The structure of **6d** was determined by single-crystal X-ray crystallography.

Figure 1 shows a plot of the molecule with atomic labeling. For clarity, the BF_4 anion has been omitted. The thermal ellipsoids were plotted at the 50% probability level. Hydrogen atoms were included at calculated positions and were refined riding on the parent atom. Tables of bond distances and angles, least-squares planes, and positional and thermal parameters are given in the supplementary material.

As shown in Figure 1, the tellurapyrylium ring is significantly distorted from the pyrylium ring. The pyrylium ring is bent 4.2° out of plane along the O–C8 axis while the tellurapyrylium ring is bent 8.7° out of plane along the Te–C3 axis. Selected bond distances and angles are in-

Scheme II

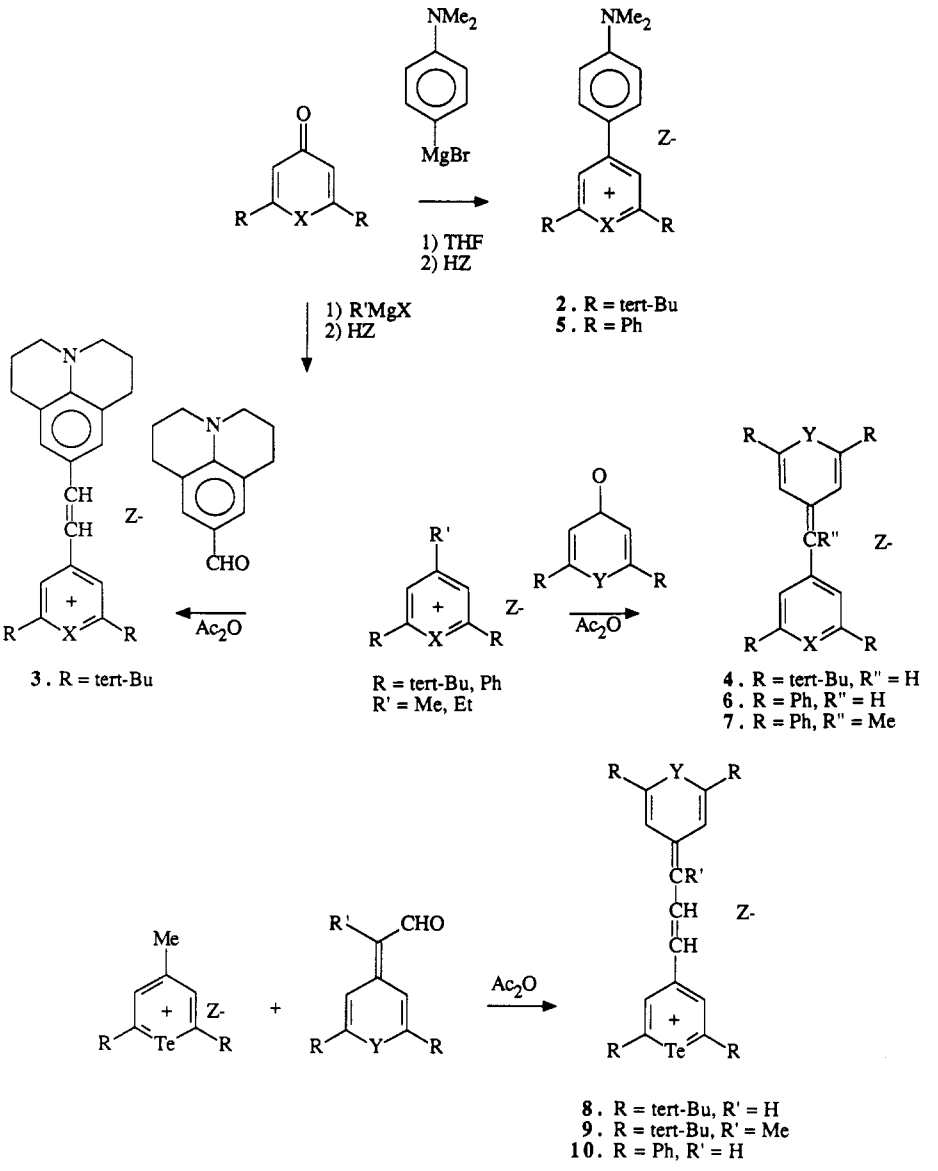

cluded in Table II. The long Te–C bond lengths relative to the C–O and C–C bond lengths make the C1–Te–C5 bond angle (94.3°) markedly different from the 120° bond angle of the C6–O–C10 atoms.

The tellurapyrylium ring of **6d** can be compared with the tellurapyranyl ring of 11.[6b] The oxidative addition

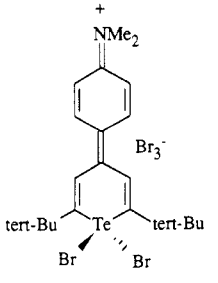

11

of bromine across the Te atom of 11 has removed the orbitals capable of π-bonding to the carbon π-framework. The Te–C bond lengths of 2.12 Å in 11 are 0.05 Å longer than the Te–C bond lengths in **6d**. With use of the numbering scheme of Figure 1, the C1–C2 and C4–C5 bonds in 11 are 0.02 Å shorter than the same bonds in **6d**. The C2–C3 and C3–C4 bonds in 11 are 0.02 Å longer than the same bonds in **6d**. With the assumption that 11 has single Te–C bonds and well-defined C–C single and double bonds, the tellurapyrylium nucleus in **6d** has a delocalized π-framework with shortened single bonds and lengthened double bonds. In the pyrylium nucleus of **6d**, the C6–C7 and C9–C10 bonds (average = 1.344 Å) are near normal double bonds but the C7–C8 and C8–C9 bonds (average = 1.422 Å) are 0.05 Å shorter than normal single bonds. The O–C6 and O–C10 bonds (average = 1.369 Å) are shortened by 0.02 Å relative to the O–C bond of 2,2′,6,6′-tetraphenylpyranylpyran (average = 1.389 Å).[4e] As one would expect from the differences in covalent radii among carbon, oxygen, and tellurium, the pyrylium ring appears to have more π-bonding from the heteroatom than does the tellurapyrylium ring as evidenced by the shortened C–C and C–O single bonds.

Electrochemical Studies. The dyes **2–10** were examined by cyclic voltammetry (CV). The electrochemical data are summarized in Table III for the 2,6-di-*tert*-butylchalcogenapyrylium nucleus and in Table IV for the 2,6-diphenylchalcogenapyrylium nucleus.

The *p*-(*N*,*N*-dimethylamino)phenyl dyes **2** and **5** and the julolyldyl dyes **3** were characterized by partially reversible oxidation waves. At scan rates of 0.5 V s^{-1} or faster, the

Table III. Redox Properties for 2,6-Di-*tert*-butylchalcogenapyrylium Dyes 2–4, 8, and 9

		$E_{ox}°$,[a] V		$E_{red}°$,[a] V		$E_{red}°'$,[a] V	
compd	solv	E_p^a	E_p^c	E_p^c	E_p^a	E_p^c	E_p^a
2a	CH_3CN	1.09	1.02	−0.57	−0.505	−1.60	
	CH_2Cl_2	0.98		−0.57	−0.50		
2b	CH_3CN	1.14	1.08	−0.64	−0.58	−1.65	
2c	CH_3CN	1.16	1.09	−0.75	−0.68	−1.70	
	CH_2Cl_2	1.35		−0.71	−0.61		
2d	CH_3CN	1.255	1.18	−0.845	−0.77		
3a	CH_3CN	0.71	0.635	−0.475			
3b	CH_3CN	0.74	0.65	−0.53			
3c	CH_3CN	0.73	0.64	−0.62			
3d	CH_3CN	0.73	0.63	−0.74			
4a	CH_3CN	1.01		−0.435	−0.37	−1.395	−1.315
	CH_2Cl_2	1.13		−0.37	−0.30	−1.39	−1.31
4b	CH_3CN	1.05		−0.485	−0.415	−1.47	−1.40
4c	CH_3CN	1.04		−0.55	−0.485	−1.53	−1.44
4d	CH_3CN	1.08		−0.62	−0.56	−1.55	
4e	CH_3CN	1.16		−0.55	−0.47	−1.545	−1.47
8a	CH_2Cl_2	0.86		−0.365	−0.28	−1.41	−1.33
8b	CH_2Cl_2	0.94		−0.45	−0.38	−1.45	−1.38
9a	CH_2Cl_2	0.82		−0.385	−0.31	−1.44	−1.35
9b	CH_2Cl_2	0.87		−0.44	−0.35	−1.53	−1.38

[a] Volts vs SCE at a platinum disk electrode with a scan rate of 0.1 V s^{-1} and 0.2 M $Bu_4N^+BF_4^-$ as supporting electrolyte.

Table IV. Redox Properties of 2,6-Diphenylchalcogenapyrylium Dyes 5–7 and 10

		$E_{ox}°$,[a] V		$E_{red}°$,[a] V		$E_{red}°'$,[a] V	
compd	solv	E_p^a	E_p^c	E_p^c	E_p^a	E_p^c	E_p^a
5a	CH_3CN	1.12	1.05	−0.355	−0.285	−1.26	−1.14
	CH_2Cl_2	1.31		−0.28	−0.20	−1.22	
5b	CH_3CN	1.20	1.11	−0.445	−0.365	−1.35	−1.27
	CH_2Cl_2	1.33		−0.35	−0.26	−1.30	
5c	CH_3CN	1.23	1.15	−0.53	−0.46	−1.40	−1.32
	CH_2Cl_2	1.40		−0.37	−0.29		
5d	CH_3CN	1.30	1.22	−0.63	−0.55	−1.61	−1.53
	CH_2Cl_2	1.48		−0.51	−0.43		
6a	CH_3CN	1.04		−0.195	−0.13	−0.985	−0.92
	CH_2Cl_2	1.19		−0.12	−0.04	−0.98	−0.90
6b	CH_2Cl_2	1.25		−0.17	−0.09	−1.05	−0.97
6c	CH_2Cl_2	1.26		−0.22	−0.14	−1.09	−1.01
6d	CH_2Cl_2	1.31		−0.28	−0.20	−1.18	−1.10
7a	CH_2Cl_2	0.74		−0.08	+0.03	−0.995	−0.92
7b	CH_2Cl_2	0.80		−0.11	−0.01	−1.04	−0.95
7c	CH_2Cl_2	0.84		−0.15	−0.07	−1.07	−0.99
7d	CH_2Cl_2	0.85		−0.20	−0.13	−1.14	−1.06
7e	CH_2Cl_2	0.88		−0.15	−0.05	−1.09	−0.90
10a	CH_2Cl_2	0.85		−0.10	−0.02	−0.99	−0.91
10b	CH_2Cl_2	0.87		−0.13	−0.05	−1.05	−0.97

[a] Volts vs SCE at a platinum disk electrode with a scan rate of 0.1 V s^{-1} and 0.2 M $Bu_4N^+BF_4^-$ as supporting electrolyte.

ratio of anodic and cathodic currents (i_p^a/i_p^c) was approximately 1 but increased as the scan rate slowed and the size of the heteroatom increased (~1.1 for **5d** to ~1.5–2 for Te-containing dyes **2a**, **3a**, and **5a** at 0.1 V s^{-1}). The other chalcogenapyrylium dyes were characterized by irreversible oxidations.

The first reduction wave for the julolyldyl dyes **3** was irreversible. The first reduction waves for all of the other dyes were reversible with i_p^c/i_p^a = 1.0 and ΔE_p of ~60 mV at slow (0.02–0.1 V s^{-1}) scan rates in both acetonitrile and dichloromethane. A plot of i_a for oxidations or i_p for reductions against the square root of scan speed was linear for all compounds across a range of 0.02–0.5 V s^{-1} (correlation coefficient >0.99) as expected for a diffusion-controlled electrode process.[8]

The second reduction waves for the 2,6-diphenylchalcogenapyrylium dyes **6**, **7**, and **10** were reversible in both acetonitrile and dichloromethane with $i_p^c/i_p^a \approx$ 1.0–1.15 and with ΔE_p approaching 60 mV at slow scan speeds. The second reduction waves for dyes **4**, **5**, **8**, and **9** were partially reversible with i_p^c/i_p^a between 1.1 and 1.7, even at scan rates of 0.5 V s^{-1}. Dye **4d** gave an irreversible second reduction wave, even at fast scan rates, as did the dimethylaniline dyes **2**.

The one-electron nature of the redox waves associated with the chalcogenapyrylium dyes was demonstrated by controlled potential electrolysis in a standard divided cell. Reduction of **2a** and **6a** required 1.09 and 1.05 faradays/mol, respectively, to reach current plateaus at −0.65 and −0.25 V (vs SCE), respectively. Oxidation of the electrolyzed solutions regenerated the starting dyes as evidenced by absorption spectroscopy and cyclic voltammetry.

Discussion

The Relationship of Redox Potentials with ϵ_{HOMO} and ϵ_{LUMO}. The electrochemical half-wave potential is the voltage required to reduce or oxidize a compound under equilibrium conditions. This requires that forward electron transfer at the electrode surface be equal to the rate of reverse electron transfer.[11] Thus, in equilibrium with the HOMO of the chalcogenapyrylium cation at $E_{ox}°$ is the singularly occupied molecular orbital (SOMO) of the radical dication (Scheme I) and in equilibrium with the LUMO of the chalcogenapyrylium cation at $E_{red}°$ is the SOMO of the neutral radical. Further reduction of the neutral radical gives the chalcogenapyranyl anion (Scheme I). At $E_{red}°$ for this couple, the SOMO of the neutral radical is in equilibrium with the HOMO of the anion.

Reversible polarographic half-wave potentials ($E_{ox}°$ and $E_{red}°$) of the chalcogenapyrylium dyes have been related to the energy of the highest occupied (ϵ_{HOMO}) and lowest unoccupied (ϵ_{LUMO}) molecular orbitals by the following equations[1a,13,14]

$$E_{ox}° = -\epsilon_{HOMO}(\text{solvent}) + C \quad (3)$$

$$\epsilon_{HOMO}(\text{solvent}) = -\text{IP} + \Delta E_{sol}^{R-} \quad (4)$$

$$E_{red}° = -\epsilon_{LUMO}(\text{solvent}) + C \quad (5)$$

$$\epsilon_{LUMO}(\text{solvent}) = \text{EA} + \Delta E_{sol}^{R+} \quad (6)$$

The term C is a constant which includes the potential of the reference electrode on an absolute scale.[14] The solvation terms ΔE_{sol}^{R-} and ΔE_{sol}^{R+} are the differences in real solvation energies between the reduced and oxidized forms of the chalcogenapyrylium nuclei and the nuclei in the gas phase. EA and IP are the gas-phase molecular electron affinity and ionization potential, respectively. The potential of the reference electrode will cancel out when the chalcogenapyrylium nuclei are compared to one another. Furthermore, within a series of dyes where structurally only the heteroatom is changing, the solvation terms should be quite similar such that solution values should give the same relative ordering of energy levels as one would expect in the gas phase.

Presumably, the relative energy of the HOMO levels of the chalcogenapyrylium dyes can be calculated directly by the differences in oxidation potentials among the systems. Similarly, the LUMO levels for the dyes in the solvent employed are obtained directly from the differences in reduction potential.

One caution to be noted with eq 3–6 is that solution redox values are determined on a much slower time scale

(13) (a) Maccoll, A. *Nature (London)* **1949**, *163*, 178. (b) Hoijtink, G. H. *Recl. Trav. Chim. Pays-Bas* **1958**, *77*, 555.
(14) Loutfy, R. O.; Sharp, J. H. *Photogr. Sci. Eng.* **1976**, *20*, 165 and references cited therein.

than gas-phase ionization potentials and electron affinities. While the solution redox values measure the adiabatic energy gap in solution between the open- and closed-shell species, the gas-phase ionization potentials (IP) and electron affinities (EA) are determined by vertical, nonadiabatic processes.[10,15,16] Unless relaxation energies are identical throughout the series of dyes studied, relative HOMO and LUMO orderings determined by eq 3–6 will be in error by differences in relaxation energy. The literature contains examples of both very good correlations between values of $E°$ and IP[14,15] and poor correlations of $E°$ and IP.[16] In many cases, good correlations have come from rigid molecules where the open-shell species is structurally quite similar to the closed-shell species[14,15] while the poor correlations have come from molecules that undergo significant geometry changes between the open- and closed-shell species.[16] As shown in the X-ray structure of **6d** (Figure 1), the chalcogenapyrylium nuclei are not planar and differences in geometry might be expected in the opened-shell and closed-shell species.

Nelsen, Peacock, and Weisman[16] have summarized the differences between rigid and nonrigid systems. In rigid systems where little reorganization occurs upon oxidation or reduction, the adiabatic gas-phase oxidation potential and the gas-phase reduction potential should be nearly identical with nonadiabatic values of IP and EA in the same systems such that eq 7 and 8 should hold. Although experimental values of IP and EA have not been obtained for the chalcogenapyrylium nuclei, theoretical methods should allow a good approximation of trends in the HOMO and LUMO energy levels in these systems in the gas phase where according to Koopmans' theorem[10]

$$E_{ox}°(\text{gas}) = \text{IP} = -\epsilon_{\text{HOMO}} \quad (7)$$

$$E_{red}°(\text{gas}) = \text{EA} = \epsilon_{\text{LUMO}} \quad (8)$$

In systems where significant geometry changes occur between the open-shell species of the same geometry as the closed-shell species (vertical or nonadiabatic ionization) and the open-shell species with relaxed geometry (adiabatic ionization), electrochemical $E°$ measures the adiabatic energy gap between the open- and closed-shell species in solution.[16] The gas-phase oxidation and reduction potentials, on an absolute scale, are now equivalent to the adiabatic ionization potential (IP_a) and electron affinity (EA_a), respectively. Values of IP_a and EA_a in the gas-phase can be approximated by theoretical methods by examining the energy differences between the closed-shell and open-shell species according to the definitions of eq 9. The correlation of these values with the solution redox values should then be possible.

$$EA_a \text{ or } IP_a = \Delta\text{SCF} = H_f(\text{products}) - H_f(\text{reactants}) \quad (9)$$

Experimentally, information about the difference between ϵ_{HOMO} and ϵ_{LUMO} can be gained from the absorption spectra of the chalcogenapyrylium compounds. The absorption of a photon is a very rapid, nonadiabatic process.[12] Although, to a first approximation, the difference in energy between the HOMO and LUMO should give the energy necessary to reach the first excited state, a more accurate representation of this energy is given by the self-consistent-field (SCF) model, in which an orbital energy corresponds to the energy of an electron which feels the field of the nuclei as well as the time-averaged fields of the other electrons.[10b] The energy of the first excited state, E_{S1}, can be related in the gas phase to the HOMO and LUMO levels by the following equation[10b]

$$E_{S1} = \epsilon_{\text{HOMO}} - \epsilon_{\text{LUMO}} - J_{12} + 2K_{12} \quad (10)$$

In eq 10, J_{12} is the Coulomb repulsion integral and K_{12} is the exchange integral. The "$2K_{12} - J_{12}$" term represents the difference in energy of the LUMO in the ground-state closed-shell configuration with the energy of the LUMO with occupancy by one electron after excitation.

The energy of the first electronic transition for the chalcogenapyrylium nucleus (the absorption maximum) is added to ϵ_{HOMO} to give the absolute level of E_{S1}. As shown in eq 3 and 4, ϵ_{HOMO} can be approximated by $E_{ox}°$ and the absolute level of ϵ_{HOMO} can then be approximated by incorporating the Fermi level of the reference electrode (for SCE in CH_3CN, −4.38 eV).[14] The difference in energy between E_{S1} and $E_{red}°$ represents the "$2K_{12} - J_{12}$" term plus the relaxation energies (including solvation) between the adiabatic and nonadiabatic HOMO and LUMO levels.

It should be possible to compare the chalcogen effects as they relate to eq 3–9 with respect to the chalcogenapyrylium nuclei. We shall first consider the experimental results in this context and shall then treat the theoretical results.

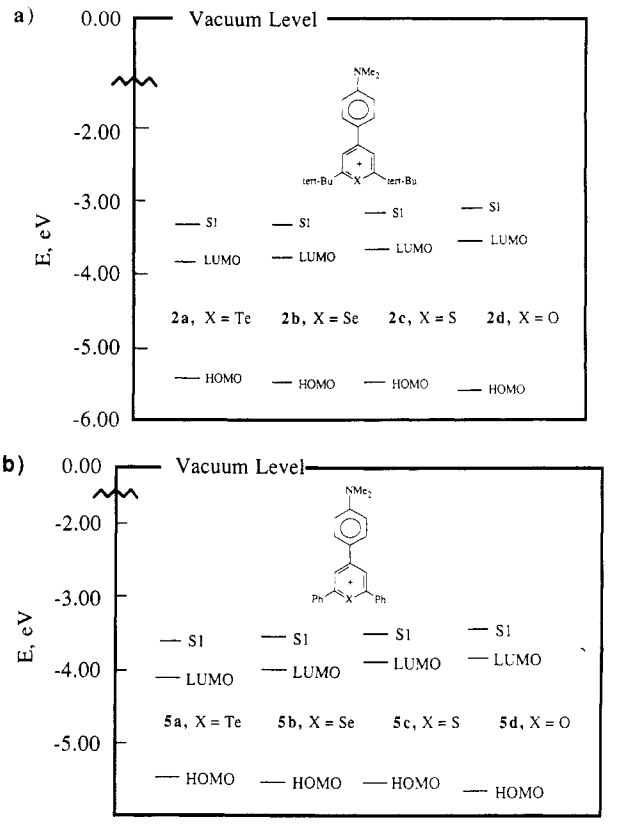

Figure 2. a. Absolute position of singlet (S_1) and electrochemical oxidation (HOMO) and reduction (LUMO) potentials for 2,6-di-*tert*-butyl-4-(4-(dimethylamino)phenyl)chalcogenapyrylium dyes **2**. b. Absolute position of singlet (S_1) and electrochemical oxidation (HOMO) and reduction (LUMO) potentials for 2,6-diphenyl-4-(4-(dimethylamino)phenyl)chalcogenapyrylium dyes **5**.

Heteroatom Effect on Electronic Absorption Spectra. The difference in E_{S1} and $E_{red}°$ is shown in Figure 2 for the dyes **2** and **5** with reversible oxidation and reduction potentials. In the 2,6-di-*tert*-butylchalcogenapyrylium dyes **2**, the "$2K_{12} - J_{12}$" terms are nearly

(15) (a) Gassman, P. G.; Yamaguchi, R. *J. Am. Chem. Soc.* **1979**, *101*, 1308. (b) Miller, L. L.; Nordblom, G. D.; Mayeda, E. A. *J. Org. Chem.* **1972**, *37*, 916. (c) James, T. H. *The Theory of the Photographic Process*; Macmillan: New York, 1977; pp 212–213 and references cited therein.

(16) Nelsen, S. F.; Peacock, V.; Weisman, G. R. *J. Am. Chem. Soc.* **1976**, *98*, 5269.

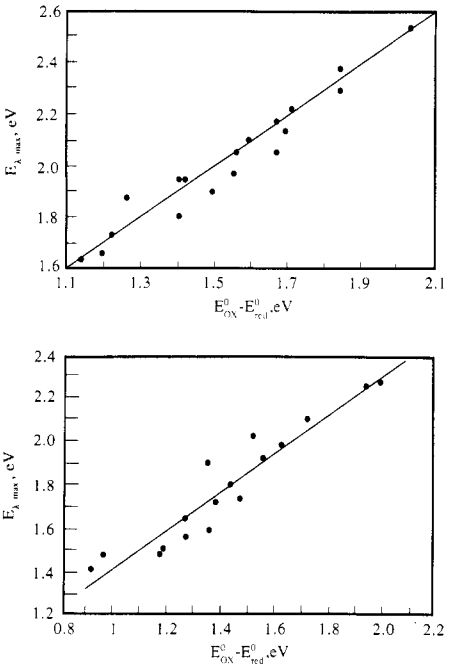

Figure 3. a. Plot of CV-determined HOMO – LUMO gaps for **2–10** as a function of the energy of corresponding absorption maxima in acetonitrile. b. Plot of CV-determined HOMO – LUMO gaps for **2–10** was a function of the energy of the corresponding absorption maxima in dichloromethane.

identical (0.51–0.52 eV). In the 2,6-diphenyl-4-(4-(dimethylamino)phenyl)chalcogenapyrylium dyes, this term has a slightly larger range (0.44–0.54 eV). The sum of the "$2K_{12} - J_{12}$" term plus the relaxation energy term appears to be nearly constant for all heteroatoms in the chalcogenapyrylium dyes. This suggests that the HOMO – LUMO gap should be directly proportional to the energy of the absorption maximum (E_{S1}).

The narrowing of the HOMO – LUMO gap in the chalcogenapyrylium dyes as the heteroatom changes from oxygen to sulfur to selenium to tellurium is suggested by the sequential bathochromic shifts observed in the absorption spectra. The differences between $E_{ox}°$ and $E_{red}°$ in solution redox potentials of the chalcogenapyrylium dyes can be compared with the energy of the first electronic transition as shown in Figure 3a in acetonitrile and in Figure 3b in dichloromethane for all the dye classes in this study with the exception of the methyl-substituted dyes **7**. Where reversible redox potentials were not available, peak potentials were used as an approximation of $E_{ox}°$ or $E_{red}°$. In acetonitrile, plotting the energy of the absorption maximum as a function of the difference between oxidation and reduction potentials gave a slope of 0.970 with an intercept of 0.53 and a correlation coefficient of 0.97. In dichloromethane, the same plot gave a slope of 0.887 with an intercept of 0.53 and a correlation coefficient of 0.97.

The intercepts in the plots shown in Figure 3 represent the weighted average of all the "$2K_{12} - J_{12}$" terms plus the relaxation energies (if any) between the adiabatic and nonadiabatic HOMO and LUMO levels. The values of this term are essentially identical in both acetonitrile and dichloromethane. Furthermore, the average values are very close to the values determined for dyes **2** and **5** in acetonitrile where both oxidation and reduction gave reversible couples.

The dyes **7** were omitted from Figure 3b since as a group the data points associated with these dyes lay more than two standard deviations off the line. The correlation of the difference in oxidation and reduction potentials of **7a–e** with the energy of their absorption maxima gave a slope of 0.89 with a correlation coefficient of 0.99. The intercept for this correlation was 0.79 eV which is significantly different than the 0.53 eV intercept determined for the other dyes. If one assumes that the "$2K_{12} - J_{12}$" term for the dyes **7** should be similar to the other dyes, then the difference in the two intercepts represents differences in adiabatic reorganization energies between the dyes **7** and the other dyes of this study.

Redox Studies. The Heteroatom Effect with Respect to the Chalcogenapyrylium Nucleus. Since the redox potentials in the chalcogenapyrylium dyes reflect thermodynamic differences between the open- and closed-shell species, one should be able to evaluate the relative contributions of σ- and π-effects from the heteroatoms to the stability of the species involved. The active methyl compounds **12–15**, which were used in the

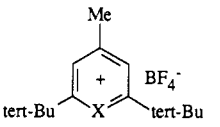

12, X = Te
13, X = Se
14, X = S
15, X = O

preparation of dyes **3** and **4**, were chosen as model systems for the parent chalcogenapyrylium nuclei. All four of these compounds oxidized at potentials more positive than +2.6 V (vs SCE) in acetonitrile and are reduced irreversibly (E_p^c = –0.51, –0.58, –0.69, and –0.76 V (vs SCE) for **12–15**, respectively). The irreversible nature of the reductions under our CV conditions is not surprising since pyranyl radicals from simple pyrylium systems have a tendency to dimerize.[17] In forming the dyes **2–10**, the parent chalcogenapyrylium nuclei have been substituted by a heteroatom-containing fragment. The presence of this fragment allows oxidation potentials to be observed in both acetonitrile and dichloromethane for these dyes.

The electrochemical data from Tables III and IV is presented in Table V as energy differences (in kcal/mol) from one heteroatom to another within each dye series. The LUMO levels as defined in eq 5 and 6 in each series of dyes are higher in energy in the order O > S > Se > Te while the HOMO levels as defined by eq 3 and 4 are higher in energy in the order Te > Se > S > O (Table V). From a strictly σ-inductive argument,[18] the chalcogenapyrylium dyes oxidizing at the least positive potential (the tellurium analogues) should reduce at the most negative potential while the most difficult to oxidize (at the most positive potential, the oxygen analogues) should be the easiest to reduce (at the least negative potential). In fact, the easiest dyes to oxidize are also the easiest to reduce suggesting that σ-donation is less important than π-donation.

The chalcogenapyrylium dyes are Hückel 6π aromatic systems[7,8] with the degree of aromatic stabilization being a measure of the effectiveness of π-overlap between the heteroatom and the carbon π-framework. In these systems, the HOMO orderings are consistent with the aromaticity of the chalcogenapyryliums being O > S > Se > Te with

(17) Pragst, F.; Ziebig, R.; Seydewitz, U.; Driesel, G. *Electrochim. Acta* **1980**, *25*, 341.

(18) The relative σ-inductive effects of the chalcogens can be inferred from the ionization potentials, I_p, or the electronegativities, X, for the heteroatoms. All values of I_p are taken from: Moore, C. E. *Natl. Bur. Stand. Circ. (U.S.)* **1949**, *1*, *No. 467*; **1952**, *2*, *No. 467*; **1958**, *3*, *No. 467*. For O, I_p = 13.614 eV: for S, I_p = 10.357 eV; for Se, I_p = 9.75 eV; for Te, I_p = 9.01 eV. All values of X are Mullay values and are taken from: Mullay, J. *J. Am. Chem. Soc.* **1984**, *106*, 5842. For O, X = 3.15; for S, X = 2.49, for Se, X 2.37; for Te, X = 2.09.

Table V. Relative HOMO and LUMO Levels for Chalcogenapyrylium Dyes and Related Species As Determined by Cyclic Voltammetry

species	relative HOMO[a] level, kcal/mol	relative LUMO[b] level, kcal/mol
	4.0 (**2a** > **2d**), 4.3 (**5a** > **5d**)	6.4 (**2d** > **2a**), 6.6 (**5d** > **5a**)
	2.7 (**2b** > **2d**), 2.6 (**5b** > **5d**)	4.7 (**2d** > **2b**), 4.5 (**5d** > **5b**)
	2.3 (**2c** > **2d**), 1.7 (**5c** > **5d**)	2.2 (**2d** > **2c**), 2.3 (**5d** > **5c**)
	8.5 (**5d** > **5a**)	
	6.3 (**5d** > **5b**)	
	5.1 (**5d** > **5c**)	
	2.9 (**6a** > **6d**)[c]	4.3 (**4d** > **4a**), 3.9 (**6d** > **6a**), 3.4 (**7d** > **7a**)
	1.5 (**6b** > **6d**)[c]	3.4 (**4d** > **4b**), 2.7 (**6d** > **6b**), 2.6 (**7d** > **7b**)
	1.2 (**6c** > **6d**)[c]	1.8 (**4d** > **4c**), 1.5 (**6d** > **6c**), 1.3 (**7d** > **7c**)
	4.7 (**4d** > **4a**), 4.9 (**6d** > **6a**), 3.5 (**7d** > **7a**)	
	2.8 (**4d** > **4b**), 3.2 (**1d** > **6b**), 2.6 (**7d** > **7b**)	
	1.6 (**4d** > **4c**), 2.2 (**6d** > **6b**), 1.7 (**7d** > **7c**)	

[a] Energy relative to most positive potential in series = 0.0 kcal/mol. [b] Energy relative to least negative potential in series = 0.0 kcal/mol. [c] Values derived from an irreversible oxidation.

oxygen being the best π-donor and tellurium, the poorest. The redox data are in agreement with the X-ray structural data for **6d** with respect to the relative amount of π-donation from the heteroatom where averaging of C–C single and double bonds is greater in the pyrylium nucleus of **6d** than in the tellurapyrylium nucleus.

The relative orderings of $E_{ox}°$ for the chalcogenapyrylium dyes are in the order expected for σ-contributions to stability, as well.[18] The tellurapyrylium nucleus should oxidize at less positive potentials than the pyrylium nucleus.

The oxidations of dyes **2** and **5** are reversible allowing a comparison of the chalcogenapyrylium and the radical dication states. Structurally, the radical dications resemble a chalcogenapyrylium-substituted aniline radical cation. Thus, the electron-donating ability of the chalcogenapyrylium groups as substituents is reflected in the oxidation of the chalcogenapyrylium dyes to the radical dications. By this analysis, the tellurapyrylium nucleus is the best electron donor while the pyrylium nucleus is the poorest.

Heteroatom Effect on Radical Stability in the Chalcogenapyranyl Radicals. Reduction of the chalcogenapyrylium dyes produces the chalcogenapyranyl radicals. In the dye series **4**–**10**, with reversible second reduction waves, the susceptibility of the chalcogenapyranyl radicals both to reversible oxidation and to reversible reduction can be examined. Of particular interest, again, are the π-donating vs σ-donating abilities of the chalcogen atoms with respect to the pentadienyl carbon framework.

Oxidation of the chalcogenapyranyl radicals would give the Hückel aromatic chalcogenapyrylium species while the reduction of the radicals would give the antiaromatic chalcogenapyranyl anions. Oxidation of the radical as determined by $E°$ for the cation/neutral radical couple is increasingly positive in the order O < S < Se < Te while reduction of the radical as determined by $E°$ for the radical/anion couple is increasingly negative in the order Te < Se < S < O. These trends are exactly those expected if the π-donating ability of the chalcogen were the dominant heteroatom effect within the pyrylium (pyranyl) nucleus and are opposite to those expected if σ-inductive effects were important. The cation is stabilized by increased π-overlap while the anion is destabilized.

Solvent Effects. Solvent effects are evident upon changing the dielectric constant of the solvent as indicated in Table I for absorption maxima in dichloromethane and acetonitrile. The solvent with higher dielectric constant (CH_3CN) gives a blue shift relative to the lower dielectric solvent. The solvent effect has been explained in terms of the higher dielectric constant solvent stabilizing the polar ground state more than the nonpolar first excited singlet state, leading to a hypsochromic shift.[5a,19]

Substituent Effects. As can be seen from Table I, the absorption maxima for the chalcogenapyrylium dyes are sensitive to substituent effects from substituents in the 2- and 6-positions. From the redox potentials listed in Tables III and IV, oxidation potentials for the chalcogenapyrylium dyes do not change much with the substitution of phenyl groups for *tert*-butyl groups. Reduction potentials are much more sensitive to substituents.

Dye **16** is a hybrid structure of **4a** and **6a** with both *tert*-butyl and phenyl substituents. As one might expect,

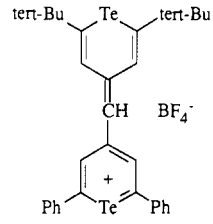

16

the absorption maximum of **16** in CH_2Cl_2 (745 nm) is between that of **4a** (710 nm) and that of **6a** (760 nm). The redox potentials of **16** are between those of **4a** and **6a**, as well, with E_p^a of +1.15 V (vs SCE) and $E°'$ for reduction of –0.14 V and $E°''$ for reduction of –1.01 V in CH_2Cl_2. The differences in the oxidation potentials of the three dyes are much smaller than the differences in reduction potentials.

Increasing the conjugation in the hydrocarbon backbone exerts little influence on the LUMO energy levels of the chalcogenapyrylium dyes but raises the HOMO energy levels substantially. Comparing dyes **2** with **3**, **4** with **8**, and **6** with **10** shows approximately a 0.3 V change in oxidation potential upon the addition of a double bond while the change in reduction potential is less than 0.1 V.

The most unusual substituent effects are observed in comparing dye classes **6** and **7** with dye classes **8** and **9**. The chalcogenapyrylium dyes **7**, substituted with a methyl group on the methine bridge, show a large bathochromic shift in absorption maxima relative to the unsubstituted derivatives **6** (Table I). The reduction potentials for these two classes of dyes are essentially identical while the oxidation potentials are much less positive in the methyl-substituted series (Table IV).

The magnitude of the bathochromic shift observed between dyes **6** and **7** as well as the magnitude of the differences in oxidation potential seemed quite large for the inductive effect of a methyl group. Substitution of a methyl for hydrogen at a similar position in the trimethine dyes **8** and **9** gave much smaller bathochromic shifts in absorption maxima (Table I) and much smaller changes in oxidation potential (Table III). As in **6** and **7**, methyl substitution had little effect on reduction potentials in **8** and **9**. One might expect the monomethine dyes to be

(19) Kosower, E. M. *J. Am. Chem. Soc.* **1958**, *80*, 3253.

Table VI. MNDO Determined HOMO and LUMO Levels for Model Compounds 17–24 and Experimental Absorption Maxima Energies for Dyes 2c, 2d, 5c, 5d, and 25–31

model compd	ϵ_{HOMO}, eV	ϵ_{LUMO}, eV	$\epsilon_{HOMO} - \epsilon_{LUMO}$, eV	compd	λ_{max}, nm	$E_{\lambda_{max}}$, eV
17	−15.76	−6.69	9.07			
18	−15.76	−7.14	8.62			
19	−11.868	−5.620	6.248	**2d**	495	2.507
				5d	550	2.256
20	−11.950	−5.921	6.029	**2c**	543	2.285
				5d	592	2.096
21	−12.021	−5.702	6.319	**25**	480	2.585
				28	545	2.277
22	−12.038	−5.955	6.083	**26**	526	2.359
				29	585	2.121
23	−12.091	−6.245	5.846	**27**	577	2.151
				30	622	1.995
24	−12.051	−5.692	6.359	**31**	614	2.021

much more sensitive to steric effects (methyl substitution for hydrogen) than the trimethine dyes. Relief of strain might increase dihedral angles in the dyes which would give large bathochromic shifts by raising the energy of the HOMO. Furthermore, one might expect geometry changes in the open-shell and closed-shell species under adiabatic conditions.

Interestingly, the difference in energy of the intercept of the correlation of the oxidation and reduction potential with the energy of the absorption maximum with the "$2K_{12} - J_{12}$" term for the dyes **7** relative to the other phenyl-substituted chalcogenapyrylium dyes (0.26 eV) is of the same magnitude as the differences in $E_{ox}°$ (0.42–0.46 eV). If this difference were due to steric effects in the adiabatic reorganization energies, a quantitative assessment would be desirable.

We next turned to a theoretical examination of the chalcogenapyrylium nuclei. In particular, we were interested in exploring the steric influences of the methyl substituent in dyes of structure **7** and in evaluating IP's and EA's under both nonadiabatic and adiabatic conditions.

Theoretical Studies. The parent chalcogenapyrylium nuclei can be viewed as being constructed by the combination of a pentadienyl cation with a chalcogen atom as shown in eq 11. The chalcogenapyrylium rings are Hückel

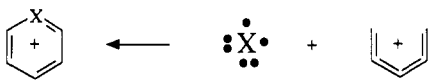

(11)

6π aromatic systems with the positive charge delocalized on the heteroatom, C-2, C-4, and C-6. Calculations have shown that the π-orbitals of 2,4,6-triphenylpyrylium and 2,4,6-triphenylthiapyrylium nuclei are benzene-like.[7,8] The HOMO and LUMO in these systems are located in the π-framework and are not localized on the heteroatom lone pair of electrons, because of the nodal properties of the occupied e_2 benzene-like molecular orbitals.[7,8]

The effect of the chalcogen atoms on the energies of the HOMO and LUMO will be determined by the weighted contributions of these atoms to the HOMO and LUMO. We initially investigated only the model pyrylium and thiapyrylium compounds **17–24** (Chart I) using MNDO[9] as implemented in the MOPAC program,[20] since suitable parameters are not available for Se and Te. The HOMO and LUMO energies in these systems, the HOMO – LUMO gap ($\epsilon_{LUMO} - \epsilon_{HOMO}$), and the energy of the absorption maxima of the 2,6-di-*tert*-butyl-substituted analogues **2d**, **2c**, and **25–27** and of the 2,6-diphenyl analogues

(20) Program 4558 *QCPE*, Indiana University, Bloomington, IN.

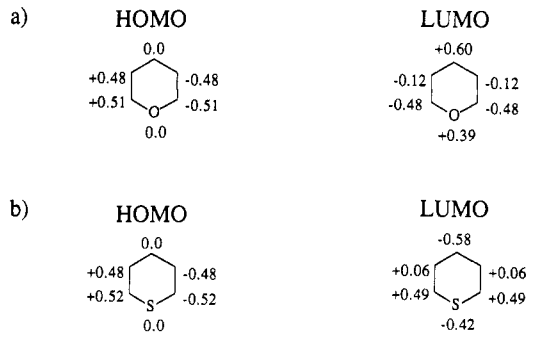

Figure 4. HOMO and LUMO coefficients for (a) model pyrylium **17** and (b) model thiapyrylium **18**.

Table VII. Symmetry and Orbital Energies of the π-Orbitals for Model Compounds 17 and 18

orbital	symmetry	E_π 12	E_π 13
π_6	S	−3.74	−3.73
π_5	A	−5.82	−5.60
π_4 (LUMO)	S	−6.69	−7.14
π_3 (HOMO)	A	−15.76	−15.76
π_2	S	−16.93	−16.21
π_1	S	−22.08	−19.16

5d, **5c**, and **28–31** in CH_2Cl_2 are compiled in Table VI.

The Parent Chalcogenapyrylium Nuclei. Figure 4 shows the coefficients for the HOMO and LUMO of the parent pyrylium and thiapyrylium rings. The π-orbitals are benzene-like with the same molecular orbital symmetries. The energies of the π-orbitals in the pyrylium and thiapyrylium rings are nearly identical as shown in Table VII. The HOMO in each system is characterized by a nodal plane through the heteroatom and the C atom at the 4-position. One would expect little contribution from the heteroatom to the energy of the HOMO, and, as a consequence, the energy of the HOMO is almost identical in each system. Experimental oxidation potentials then might be expected to be very similar as well in simple systems. The LUMO in each system is characterized by a large contribution from the heteroatom such that changing the heteroatom in these systems would be expected to affect the LUMO energy level.

The coefficients listed in Figure 4 are in excellent agreement with those reported for CNDO calculations of pyrylium systems[7] and for Hückel MO calculations of pyrylium and thiapyrylium systems.[8] Energy levels in Table VII are correspondingly similar between MNDO[9] and the CNDO and Hückel calculations for these systems.

The Chalcogenapyrylium Dye Nuclei. Figure 5 shows the coefficients of the HOMO and LUMO for the 4-(4-(dimethylamino)phenyl)-substituted nuclei **19** and **20**, and Figure 6 shows the coefficients of the HOMO and LUMO for **21–23**. The heteroatoms in these systems contribute to both the HOMO and LUMO. Changing the chalcogen atom in these systems would be expected to influence the energy level of both the HOMO and LUMO. The MNDO[9] calculations predict that, in the gas phase, both the HOMO and LUMO will drop in energy upon the substitution of sulfur for oxygen although the effect on the HOMO will be much less than the effect on the LUMO.

The coefficients in Figure 5 indicate that the HOMO is predominantly the aniline fragment (≈65% in both **19** and **20**) while the LUMO is predominantly (≈75% in both **19** and **20**) the chalcogenapyrylium fragment. One would expect the effects of chalcogen substitution to be more pronounced in the LUMO than in the HOMO. In agreement with this, the experimental redox potentials show

Chart I

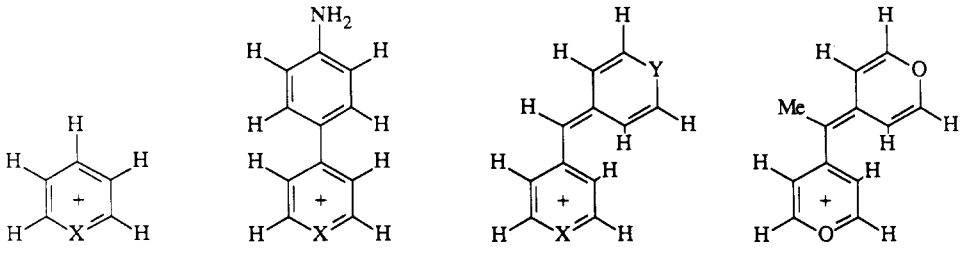

17, X = O
18, X = S

19, X = O
20, X = S

21, X = Y = O
22, X = S, Y = O
23, X = Y = S

24

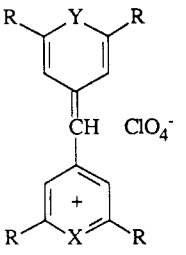

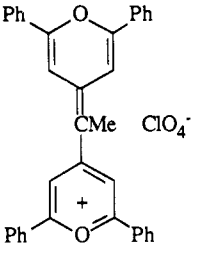

25, X = Y = O, R = tert-Bu
26, X = S, Y = O, R = tert-Bu
27, X = Y = S, R = tert-Bu
28, X = Y = O, R = Ph
29, X = S, Y = O, R = Ph
30, X = Y = S, R = Ph

31

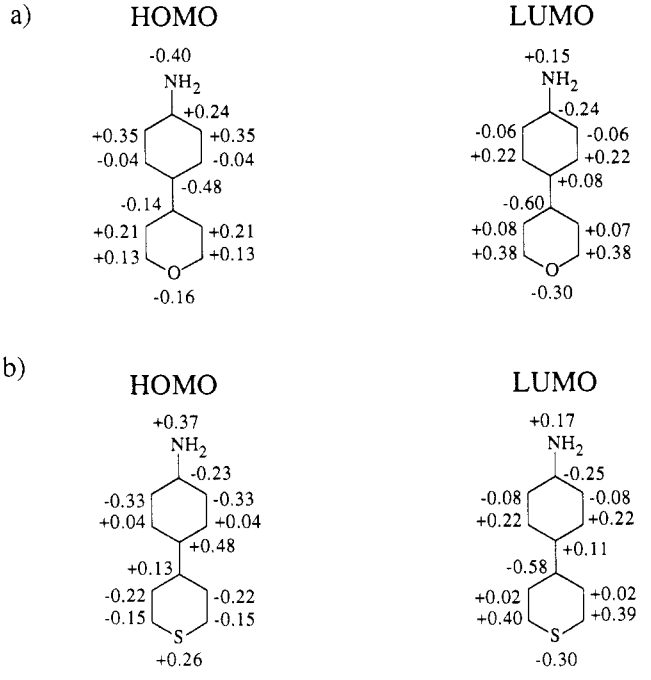

Figure 5. HOMO and LUMO coefficients for (a) model 4-(4-aminophenyl)-substituted pyrylium **19** and (b) model 4-(4-aminophenyl)-substituted thiapyrylium **20**.

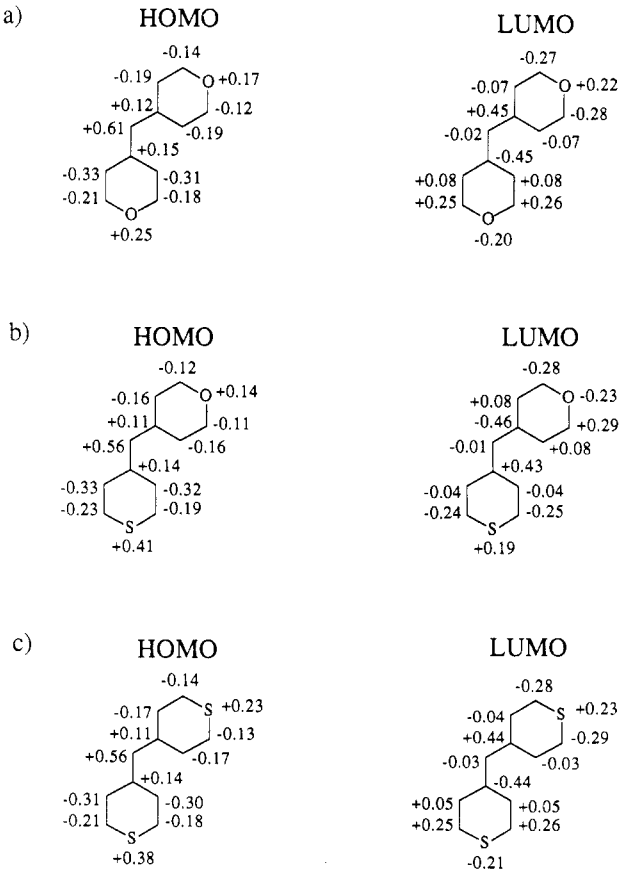

Figure 6. HOMO and LUMO coefficients for (a) model pyranylpyrylium **21**, (b) model pyranylthiapyrylium **22**, and (c) model thiapyranylthiapyrylium **23**.

much larger changes in reduction potentials than the changes in oxidation potential with chalcogen substitution.

The styryl dyes **3** show essentially identical reversible oxidation potentials although the reduction potentials follow the pattern of the other chalcogenapyrylium dyes. A modified OMEGA[21,22] procedure was used to allow a quick determination of coefficients in the model compounds **36** and **37**. The weight of the aniline moiety predominates in the HOMO (75–80%) with little contribution from the bridging carbons or the chalco-

(21) Streitwieser, A., Jr. *Molecular Orbital Theory for Organic Chemists*: Wiley: New York, 1962.

(22) McKelvey, J. M., work to be published. The α-term is a function of the Slater exponent; the β-term is a linear function of bond order; the π-term is atom-type dependent.

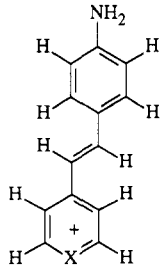

36, X = O
37, X = S

genapyrylium ring. The weight of the chalcogenapyrylium ring predominates in the LUMO (~70%) with little contribution from the aniline or bridging carbons. The coefficients at the chalcogen atom in the HOMO are 0.107 and 0.096 for **36** and **37**, respectively, while the coefficients at the chalcogen atom in the LUMO are 0.366 and 0.439 for **36** and **37**, respectively. The nitrogen coefficient is quite large in the HOMO of both **36** and **37** (0.622 and 0.637 for **36** and **37**, respectively) and quite small in the LUMO (0.111 and 0.092 for **36** and **37**, respectively). In view of this analysis, the similarity of $E_{ox}°$ in the dyes **3** is not surprising.

The weight of each chalcogenapyrylium unit in **21–23** (Figure 6) to the HOMO is comparable to the weighted contribution of the chalcogenapyrylium unit in **19** and **20** (Figure 5) to the HOMO. In **21–23**, the rest of the HOMO resides on the bridging methine carbon which is similar in weight to that of the aniline nitrogen in **19** and **20**. In the LUMO's of **21–23**, there is no contribution from the bridging methine with all of the weight of the LUMO coming from the chalcogenapyrylium units. Again, one would expect larger changes in reduction potentials than in oxidation potentials upon chalcogen substitution in **4** and **6**.

The aniline dyes **19** and **20** can be viewed as the combination of a chalcogenapyrylium nucleus with an aniline. The HOMO of these systems is predominantly the aniline moiety while the LUMO is predominantly the chalcogenapyrylium nucleus. From the coefficients in Figure 6, the monomethine dyes **21–23** can be viewed as the combination of two chalcogenapyrylium nuclei with a carbon anion. The HOMO of these systems lies on the methine carbon while the LUMO of these systems is predominantly the chalcogenapyrylium nuclei.

From Table VII, the HOMO – LUMO gap ($\epsilon_{LUMO} - \epsilon_{HOMO}$), predicted by MNDO,[9] correlates in a qualitative sense with the observed absorption spectra in both the phenyl- and *tert*-butyl-substituted derivatives. As the HOMO – LUMO gap increases in energy in the model compounds, the wavelength of the absorption maximum of the corresponding dye shifts to shorter wavelength. This correlation holds both with phenyl substituents that can conjugate with the carbon π-framework and with *tert*-butyl substituents that cannot, as shown in Figure 7 for a plot of the HOMO – LUMO gap vs the energy of the absorption maxima. The correlation coefficients for the two lines in Figure 7 are 0.994 for the 2,6-diphenyl-substituted dyes and 0.997 for the 2,6-di-*tert*-butyl-substituted dyes with slopes of 1.582 and 1.07, respectively.

The methyl substituent in **31** as well as in the other analogues **7** would be expected to exert a steric influence on the absorption maximum as well as an electronic influence. It is recognized that MNDO[9] gives energies that are too positive for crowded molecules.[23] The failure of the correlation of **24** with **31** to fit the line described in Figure 4 is not surprising. The methyl substituent in these

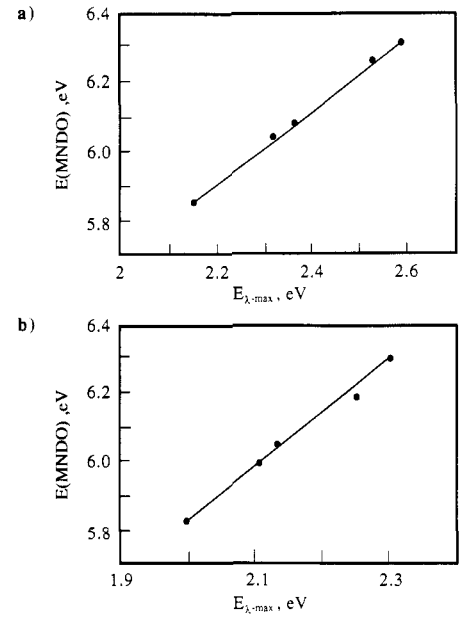

Figure 7. a. Plot of MNDO determined HOMO – LUMO gaps for **19–23** vs experimental absorption maxima energies for **2c**, **2d**, and **25–27**. b. Plot of MNDO determined HOMO – LUMO gaps for **19–23** vs experimental absorption maxima energies for **5c**, **5d**, and **28–30**.

systems will be treated independently (vide infra).

If one examines the energy levels of the HOMO and LUMO in the model systems **19–23**, two trends emerge when compared with the experimental redox potentials listed in Tables III and IV. Both experiment and theory agree that the LUMO's of the pyrylium nuclei are higher in energy than the LUMO's of the thiapyrylium nuclei. Reduction of the pyrylium nuclei occurs at more negative potentials than reduction of the corresponding thiapyrylium nuclei. However, theory and experiment do not agree with respect to the effect of heteroatom substitution on HOMO levels. In the model dyes **19–23**, MNDO[9] predicts that the HOMO's of the thiapyrylium nuclei are slightly lower in energy than the HOMO's of the pyrylium nuclei. One would expect the thiapyrylium nucleus to be oxidized at more positive potentials than the pyrylium nucleus. The experimental oxidation potentials for **2c** and **2d** and for **5c** and **5d** show exactly the opposite trend with the pyrylium nuclei being oxidized at more positive potentials than the thiapyrylium nuclei. Similarly, the oxidation potentials for the monomethine dyes **4** and **6**, even though they are irreversible, are increasingly positive in the order Te < Se < S < O.

Adiabatic Ionization Potentials and Electron Affinities. The failure of Koopmans' theorem[10] to predict the observed trends to redox potentials upon chalcogen atom substitution suggests that IP_a and EA_a are significantly different from IP and EA, respectively. We used MNDO[9] to predict ΔSCF IP's and EA's (IP_a and EA_a, respectively) incorporating, for the first time, a restricted Hartree–Fock MNDO procedure that was efficiently performed.

Table VIII contains MNDO[9] determined heats of formation (H_f) for pyrylium nucleus **9** and thiapyrylium nucleus **10** as well as their corresponding radical dications, neutral radicals, and anions in the gas phase with optimized geometry for all species. The ΔSCF values for the half-reactions shown suggest that the thiapyrylium nucleus should oxidize at less positive potentials than the pyrylium nucleus and that the thiapyrylium nucleus should reduce at less negative potentials than the pyrylium nucleus under

Table VIII. MNDO and AM1 Determined Heats of Formation (H_f in kcal/mol) and ΔSCF Values for Model Compounds 17–23 and Their Dictation Radicals, Neutral Radicals, and Anions Where ΔSCF = H_f(products) − H_f(reactants)

	H_f					
model compd	dictation radical		cation		neutral radical	anion
17[a,b]	575.15		162.69		1.10	−7.23
|ΔSCF|		412.46		161.59	8.33	
18[a,b]	562.37		209.99		39.06	15.04
|ΔSCF|		352.38		170.93	24.02	
19[b,c]	439.38		178.76		35.90	13.36
|ΔSCF|		260.62		142.86	32.54	
20[b,c]	484.58		225.72		76.63	45.32
|ΔSCF|		258.86		149.09	31.31	
19[a,d]	442.70		180.21		37.19	11.67
|ΔSCF|		262.49		143.02	25.52	
20[a,d]	490.83		226.99		76.97	40.87
|ΔSCF|		264.84		150.02	36.10	
21[a,d]	416.07		152.53		11.24	
|ΔSCF|		263.54		141.29		
22[a,d]	463.04		197.99		49.04	
|ΔSCF|		265.05		148.95		
23[a,d]	462.89		244.08		48.95	
|ΔSCF|		218.81		195.13		

[a] MNDO. [b] Optimized geometry for all species [c] AM1 using MNDO parameters for S. [d] Optimized geometry for parent cation. Dictation radical and neutral radical are constrained to the geometry of the parent cation.

adiabatic conditions. Furthermore, the thiapyranyl radical should reduce at less negative potentials than the pyranyl radical. These are the trends that are observed in the redox studies of the dyes **2–10**.

In model compounds **19** and **20**, steric repulsion among the hydrogens of the two rings would be expected to be important in determining the appropriate values of H_f for all of the species in question (the radical-dication, the parent cation, the neutral radical, and the anion). Because the nuclear repulsion terms are known to be too large in MNDO,[9,23] we used AM1[23] to determine values of H_f for the parent cations, radical dications, neutral radicals, and anions of **19** and **20**. Since AM1 has not been parameterized for sulfur, we used MNDO[9] parameters for sulfur with AM1[24] parameters for the other atoms. This assumption allows for reasonable torsional effects because of the AM1 treatment of CH–CH interactions. Furthermore, it is assumed that there will be systematic cancellation of the effect of having MNDO parameters for sulfur. The values of H_f and ΔSCF for **19** and **20** and related species are compiled in Table VIII.

With use of AM1,[23] the geometries of the parent cations (**19** and **20**) and their neutral radicals and radical-dications were fully optimized. The geometry of the cation **19** is predicted to have a nearly planar geometry with the aniline and pyrylium rings only 6° out of plane. Delocalization of the positive charge with increased bonding between the carbons connecting the two rings helps to overcome the hydrogen–hydrogen repulsion between the two rings. The HOMO of **19** is heavily weighted on the aniline ring. Oxidation of **19** to the radical dication of **19** would be expected to place a positive charge in each ring. Both charge repulsion and hydrogen–hydrogen repulsion combine with the decreased C–C bonding between the two rings to give the radical dication of **19** a 37° dihedral angle between the two planes. With the neutral radical of **19**, there is decreased C–C bond order between the two rings and no driving force for planarity from charge delocalization. Hydrogen–hydrogen repulsion gives rise to a 27° dihedral angle between the two rings. Dihedral angles were similar in the sulfur series, as well, although slightly larger in the radical dication and neutral radical (42° and 33°, respectively).

The heats of formation as determined for fully optimized geometries of **19** and **20** and their radical dications and neutral radicals using AM1[23] can be compared to MNDO[9] determined heats of formation for the same series constraining the geometries of the radical dications and neutral radicals to that of the parent cation (Table VIII). Only small differences were noted between the two values for the parent cations and neutral radicals suggesting that geometry optimization is perhaps not necessary for comparison of heats of formation for these species. However, geometry optimization significantly lowered the energy of the radical dications and the anions of these systems. With the optimized geometries using AM1,[23] the ΔSCF values now track the observed changes in redox values for **2c** and **2d** and for **5c** and **5d**.

Table VIII gives the MNDO[9] calculated heats of formation for the model dyes **21–23** and their dication radicals and neutral radicals. These values were determined by single-point calculations using the optimized geometry of the chalcogenapyrylium cations and constraining the radical dication and neutral radical to this geometry.

The ΔSCF values track the observed experimental redox values for the monomethine dyes **4** and **6** in the comparison of **21** and **23**. Substitution of sulfur for oxygen in these systems leads to less positive oxidations of the parent cation and less negative reductions of both the parent cation and the corresponding neutral radical. Replacing one oxygen in **16** by sulfur to give **17** showed little change by MNDO[9] in the ΔSCF for the cation/radical dication couple although the predicted change by MNDO[9] was not in the direction found by experiment.

The ΔSCF values predict smaller changes in the oxidation potentials than in the reduction potentials upon substitution of sulfur for oxygen. Experimentally, the changes are comparable in magnitude in both oxidation and reduction upon substitution of sulfur for oxygen (Table V). With selenium and tellurium substitution, reduction potentials change much more than oxidation potentials.

The cumulative effect on the second reduction potential by substitution of sulfur for oxygen in **19** and **20** is predicted by ΔSCF values to be slightly greater than a factor of 2 more than the effect on the first reduction potential. Experimentally, the second reduction potential in **5c** and **5d** changes by 5.1 kcal/mol upon sulfur substitution while the first reduction potential changes by 2.3 kcal/mol (Table V). Furthermore, the ΔSCF values predict that the second reduction wave in **5d** should be at more negative potentials than in **5c** as is observed.

Methyl Substituents. The chalcogenapyrylium dyes **7**, substituted with a methyl group on the methine bridge, show a large bathochromic shift in absorption maxima relative to the unsubstituted derivatives **6** (Table I). The reduction potentials for these two classes of dyes are essentially identical while the oxidation potentials are much less anodic in the methyl-substituted series (Table IV). From the coefficients shown in Figure 6 for **21–23**, a substituent change at the methine carbon would be expected to have little effect on the LUMO since the coefficient at the methine carbon is essentially 0.0. However, the

(23) Dewar, M. J. S.; Zoebisch, E. G.; Healy, E. F.; Stewart, J. J. P. *J. Am. Chem. Soc.* **1985**, *107*, 3902.

(24) Programs used for the X-ray study were part of the Structure Determination Package, SDP-PLUS V1.0, Enraf-Nonius Corp., Delft, Holland.

Table IX. AM1 Determined HOMO and LUMO Energies for Model Compounds 21 and 24 and Experimental Energies for Absorption Maxima for 28 and 31

model compd	ϵ_{HOMO}, eV	ϵ_{LUMO}, eV	$\epsilon_{HOMO} - \epsilon_{LUMO}$, eV	compd	$E_{\lambda_{max}}$, eV
21	−12.220	−5.676	6.544	28	2.277
24	−11.959	−5.662	6.297	31	2.021

coefficient at the methine carbon in the HOMO is quite large. Since the methine position is a "non-starred" position and the methyl group is an electron donor, the substitution of methyl for hydrogen would be expected to raise the energy of the HOMO leading to a bathochromic shift.

The magnitude of the bathochromic shift observed between dyes **6** and **7** as well as the magnitude of the differences in oxidation potential seemed quite large for the inductive effect of a methyl group. Substitution of a methyl for hydrogen at a "non-starred" position in the trimethine dyes **8** and **9** gave much smaller bathochromic shifts in absorption maxima (Table I) and much smaller changes in oxidation potential (Table III). As in **6** and **7**, methyl substitution had little effect on reduction potentials in **8** and **9**.

OMEGA[21,22] calculations on model trimethine dye **38** show large coefficients on the allyl termini of the bridging 3-carbon unit in the HOMO (±0.44 compared with 0.61 for the methine carbon of **21**) and negligible coefficients in the LUMO (0.05 compared with 0.02 for the bridging methine in **21**). This suggests that purely electronic

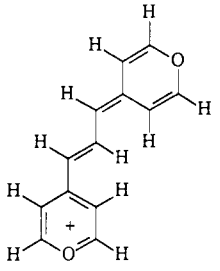

38

contributions from the methyl group might be expected to be significantly less in **7** than can be explained by the large bathochromic shift in absorption maximum and change in oxidation potential when compared with **6**.

MNDO[9] calculations on model compound **2** show the increase in HOMO energy level relative to **21** (Table VI) while the LUMO level remains relatively unchanged. The calculated change in the HOMO − LUMO gap with MNDO[9] for **21** and **24** does not correlate well with the observed changes in absorption maxima for **28** and **31**. The MNDO[9] optimized geometry of **24** shows a pronounced steric effect with the methine methyl substituent twisting the two rings out of planarity.

It was important to have good dihedral angle information for **21** and **24** because of the possible influence on both absorption maxima and oxidation and reduction potentials. As dihedral angles having low barriers are suspect by MNDO[9] in comparison with AM1,[23] model compounds **21** and **24** were fully optimized and examined by AM1. HOMO and LUMO levels and the HOMO − LUMO gap for **21** and **24** are listed in Table IX as well as energy of the absorption maxima ($E_{\lambda_{max}}$) for the experimental analogues **28** and **31**.

The 0.247 eV change in the HOMO − LUMO gap predicted by AM1[23] is nearly identical with the 0.256 eV change observed in $E_{\lambda_{max}}$ between **28** and **31**. From theory, most of this change is predicted in ϵ_{HOMO} with little change predicted in ϵ_{LUMO}. Experimentally, E_p^a for oxidation of the methylmethine dyes **7** is 0.42–0.46 eV less positive than E_p^a for their simple methine counterparts **6**. The reduction potentials of **6** and **7** differ by 0.1 V or less for corresponding pairs.

AM1[23] predicts that the two pyrylium units in **24** have opposed dihedral angles of 20° each from the plane defined by the methyl carbon, the methine carbon, and the carbon at the 4-position of the ring in question. Model compound **21** was predicted to have a nearly planar geometry. The steric influence of the methyl substituent at the methine position could significantly raise the energy of the HOMO and thus lead to longer wavelength absorption maxima and less positive oxidation potentials.

Summary and Conclusions

The contribution of the heteroatom to the stabilities of chalcogenapyrylium cations, chalcogenapyrylium radical dications, chalcogenapyranyl radicals, and chalcogenapyranyl anions has been examined experimentally by cyclic voltammetry. The redox data suggest that π-donation from the heteroatom to the carbon π-framework is important in determing the stability of the various states. The chalcogenapyranyl radicals can be oxidized to the Hückel aromatic chalcogenapyrylium nucleus or reduced to the Hückel antiaromatic chalcogenapyranyl anion. The oxidation of the radicals are increasingly positive in the order O < S < Se < Te while the reductions are increasingly negative in the order Te < Se < S < O. The decreased aromaticity and antiaromaticity as the size of the chalcogen increases would be expected with the increased covalent radii leading to less effective π-bonding.

The structure of **6d**, as determined by single-crystal X-ray crystallography, also illustrates the differences in π-bonding between the pyrylium nucleus and the tellurapyrylium nucleus. Single bonds are shorter in the pyrylium ring of **6d** relative to the tellurapyrylium ring.

The reversible cation/radical dication couples observed for dimethylanilino dyes **2** and **5** suggest that the tellurapyrylium ring, as a substituent, is more electron-donating than the other chalcogenapyrylium systems in the order Te > Se > S > O. The monomethine dyes **4** and **6** show the same trend although the oxidation potentials in these systems are irreversible.

In the chalcogenapyrylium dyes, sequential bathochromic shifts are observed from the pyrylium to thiapyrylium to selenapyrylium to tellurapyrylium nuclei within a series. A linear correlation exists between the energy of the absorption maxima of the dyes **2**–**10** and the difference in oxidation and reduction potentials. The intercept of this correlation of approximately 0.5 eV in both acetonitrile and dichloromethane corresponds to the "$2K_{12} - J_{12}$" term in determining the energy of the first singlet state.

The electron-donating ability of the chalcogenapyrylium rings as well as the contribution of the heteroatoms to chalcogenapyranyl radical stability determined in this study can be applied to other systems. The (chalcogenapyranyl)chalcogenapyran radical cations (**39**$^{\bullet+}$) can be oxidized to the dications (**39**$^{2+}$).[4] The radical cation state has an electronic structure similar to the radical dications of the chalcogenapyrylium dyes **2** and **5** (Scheme III). Table X lists values of $E°$ for the oxidation of **39**$^{\bullet+}$ to **39**$^{2+}$ for R = Ph.[4c] The value of $E°$ for this oxidation does not appear to have any correlation with the chalcogen heteroatom. The values in Table X can be "corrected" for the different electron-donating abilities of the chalcogenapyrylium nuclei to be normalized with the most electron-donating substituent (the tellurapyrylium nucleus) using the values in either Table IV or Table V. The

Scheme III

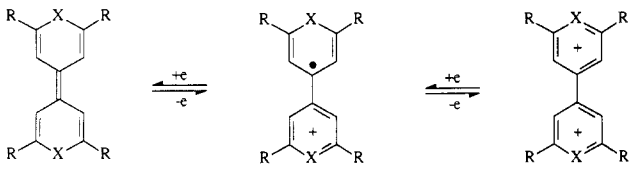

39, X = O, S, Se, Te

Table X. Oxidation Potentials ($E°'$) and Chalcogenapyrylium "Corrected" Potentials for (Chalcogenapyranyl)chalcogenapyran Radical Cations 39$^{\bullet+}$

compd	X	R	$E°'$,[a] V	corrected value[b]
39a$^{\bullet+}$	O	Ph	+0.46	+0.28
39b$^{\bullet+}$	S	Ph	+0.41	+0.30
39c$^{\bullet+}$	Se	Ph	+0.485	+0.41
39d$^{\bullet+}$	Te	Ph	+0.485	+0.485

[a] Values are taken from ref 2 and are reported vs SCE. [b] Values are corrected to the electron donating ability of the tellurapyrylium nucleus.

"corrected" values for $E°$ then follow the trends predicted for the oxidation of a chalcogenapyranyl radical with the tellurapyranyl radical oxidizing at the most positive potential and the pyranyl radical oxidizing at the least positive potential.

The MNDO[9] calculations on **17–23** suggest that the HOMO – LUMO gap in the gas phase correlates well with experimental absorption maxima obtained in solution for the chalcogenapyrylium dyes. The absorption of a photon is a rapid event[12] that proceeds without nuclear reorganization. Because of the nodal properties of the chalcogenapyrylium dyes, ionization potentials and electron affinities predicted by Koopmans' theorem[10] with the MNDO[9] calculations do not track the observed trends in the experimental redox values. Solution electrochemistry is an equilibrium process that allows both nuclear and electronic relaxation to occur in addition to solvation. Accordingly, the trends predicted by ΔSCF values calculated by MNDO[9] and AM1[23] for the open-shell (incorporating a restricted Hartree–Fock MNDO procedure) and closed-shell species, which incorporate nuclear and electronic relaxation, parallel the trends observed in the solution redox chemistry.

This study provides a good framework for the design of electron donors, electron acceptors, and dyes containing chalcogenapyrylium and/or chalcogenapyranyl groups. The heteroatoms exert a predictable influence on the reactivity or stability of adjacent ionic or radical centers. Extensions of these results to other ring systems incorporating the chalcogen atoms should be possible as well.

Experimental Section

Melting points were determined on a Thomas-Hoover melting point apparatus and are corrected. ^{1}H NMR spectra were recorded on a General Electric QE 300 instrument. IR spectra were recorded on a Beckman IR 4250 instrument. UV–visible–near-IR spectra were recorded on a Cary 17 spectrophotometer. Tellurium and selenium shot were purchased from Ventron. Tetrahydrofuran (THF) was dried over benzophenone ketyl. Solvents (Kodak Laboratory Chemicals) were dried over 3A molecular sieves before use. Solvents for electrochemistry were Baker HPLC grade and were dried over 3A sieves prior to use. Microanalyses were obtained with a Perkin-Elmer C, H, and N analyzer. Tellurium and selenium analyses were obtained by atomic absorption spectroscopy with ±1% accuracy.

The chalcogenapyranones shown in Scheme III were prepared according to ref 2 and 6b. Compounds **2a**, **8a**, **8b**, **30**, 2,6-di-*tert*-butyl-4-(formylmethylene)-4*H*-tellurapyran, and 2,6-di-*tert*-butyl-4-(formylmethylene)-4*H*-selenapyran were prepared according to ref 6b. Compounds **5a–d**, **6a–d**, and **10a–d** were prepared according to ref 6a.

Table XI. Summary of Crystal Data and Refinement Parameters for 6d

formula	$C_{35}H_{25}TeO\cdot BF_4$
mol wt	675.993
space group	$P2_1c$
cell consts at 23 (1) °C	
a, Å	13.877 (2)
b	11.344 (4)
c	19.600 (2)
β, deg	106.654 (11)
V, Å^3	2956 (2)
no. of molecules/unit cell (Z)	4
D(calcd), g cm^{-3}	1.519
cryst dimens, mm	0.20 × 0.20 × 0.36
abs coeff (μ, Mo Kα), cm^{-1}	10.57
scan technique	–2
scan rate, deg min^{-1}	2.1–20
2θ limit, deg	46
hkl range	0 to 15, 0 to 12, –21 to +21
no. of unique data measd	4103
no. of data used in refinement ($I > \sigma(I)$)	3465
no. of parameters	379
$R = \sum\|\|F_o\| - K\|F_c\|\|/\sum\|F_o\|$	0.040
$R_w = (\sum w(\|F_o\| - K\|F_c\|)^2\sum/F_o^2)^{1/2}$	0.053
$S = [(\sum w(\|F_o\| - K\|F_c\|)^2/(n_o - n_v)]^{1/2}$	1.19
wtg parameters ($w^{-1} = \alpha^2(F_o) + (pF_o)^2 + q$)	
p	0.03
q	1.0
scale factor, K	1.107 (1)
max shift in final cycle (Δ/σ)	0.04
residual electon density in final diff Fourier synthesis, e/Å^3	–0.39 to +1.15

For **2a**: ^{1}H NMR (CD_2Cl_2) δ 8.43 (s, 2 H), 8.03 (d, 2 H, J = 9 Hz), 6.95 (d, 2 H, J = 9 Hz), 3.19 (s, 6 H), 1.63 (s, 18 H).

For **5a**: ^{1}H NMR (CD_3CN) δ 8.73 (s, 2 H), 8.30 (d, 2 H, J = 9 Hz), 7.83 (m, 4 H), 7.66 (m, 6 H), 6.97 (d, 2 H, J = 9 Hz), 2.98 (s, 3 H).

For **6a**: ^{1}H NMR (CD_3CN) δ 8.14 (br s, 4 H), 7.64 (m, 12 H), 7.55 (m, 8 H), 7.28 (s, 1 H).

For **6b**: ^{1}H NMR (CD_2Cl_2) δ 8.20 (s, 2 H), 8.13 (s, 2 H), 7.76–7.50 (m, 20 H), 7.10 (s, 1 H).

For **8a**: ^{1}H NMR ($CDCl_3$) δ 8.75 (t, 1 H, J = 13.5 Hz), 7.71 (s, 4 H), 6.86 (d, 2 H, J = 13.5 Hz), 1.50 (s, 36 H).

Electrochemical Studies. A Princeton Applied Research Model 173 potentiostat/galvanostat and a Model 175 Universal programmer were used for the cyclic voltammetry studies. The working electrode was a platinum disk. Electrometric-grade tetrabutylammonium fluoroborate (Southwestern Analytical Chemicals, Inc.), recrystallized twice from ethyl acetate/pentane, was used as supporting electrolyte at 0.2 M concentration. Argon was used for sample deaeration.

X-ray Diffraction Study of 6d. The data crystal was cut to size, glued onto a thin glass rod, and used on an Enraf-Nonius CAD4 diffractometer with graphite-monochromated Mo Kα radiation. The setting angles for 25 reflections ($8.5 < \theta < 14.0°$) were refined to obtain the cell data given in Table XI. Three standard reflections were monitored every hour throughout the data collection. Data were corrected for a small (6%) loss in intensity over time. Data were also corrected for absorption (correction factors ranged from 0.84 to 1.08).[24]

The structure was solved by the heavy-atom method. The Te atom position was obtained from the Patterson map and all other non-hydrogen atoms from a subsequent difference electron density map. Although the hydrogen atoms were well-defined in a later difference map, they were input into the refinement at calculated positions and allowed to ride on the parent atoms.

There was a large positive peak (1.15 e/Å^3) in the final difference map located about 1 Å from the oxygen atom and in the plane of the pyrylium ring. This peak was present even when all the data were used (possibility of series termination errors) and when the data was corrected for absorption by using psi scan

data. Our conclusion is that this peak is real and due to a minor disorder in which about 2% of the molecules have the tellurapyrylium ring in this location. Such a small disorder might be detected for the much heavier Te atom but not for the lighter oxygen and carbon atoms. Indeed, disorder is not evident in the temperature factors for oxygen and the adjacent carbon atoms. Refinement including a Te atom with occupancy of 0.02 (B_{iso} = 4.0) at the position near the large residual peak did not cause a significant change in the oxygen atom position, so these calculations were not retained.

Molecular Orbital Procedures. In this study it was necessary to evaluate molecular geometries and heats of formation both for closed-shell, singlet molecules, and also for open-shell, radical doublets using the MNDO[9] and AM1[23] formalisms found in the MOPAC[20] program. All computations were carried out by using the default convergence criteria in the self-consistent-field procedures and in the geometry searches.

Special attention was paid, however, to the computations for the radical doublets. It is routinely possible to perform these calculations by using the half-electron procedure, wherein the energy of an open-shell molecule is derived through a connection to a closed-shell calculation, and by the conventional unrestricted Hartree–Fock procedures. We found, however, that the half-electron procedure was slower than we wished. It was also desired to perform the calculations without the usual quartet, sextet, and higher states contamination of doublet states by using the UHF procedure. A new SCF procedure that gives a wave function that is a proper eigenfunction of S^2 has been installed in MOPAC in order to alleviate these problems. This procedure was found capable of reproducing MINDO/3 results (the general coupling operator method) reported by Dewar et al. We have found this new procedure to be only about 20% slower than the usual THF scheme upon which it is based and to be about 4–6 times faster than the half-electron procedure found in MOPAC. So far, few convergence difficulties have been encountered. The details of this method will be reported elsewhere.

Preparation of 2,6-Di-*tert*-butyl-4-(4-(dimethylamino)-phenyl)selenapyrylium Perchlorate (2b). A mixture of 1.7 g (8.0 mmol) of *p*-bromo-*N*,*N*-dimethylaniline and 0.20 g (8 mmol) of Mg turnings in 20 mL of dry THF was refluxed under nitrogen until the Mg turnings disappeared. The solution was cooled to ambient temperature, and a solution of 2,6-di-*tert*-butylselenapyranone (1.41 g, 5.0 mmol) in 15 mL of dry THF was added dropwise. The mixture was heated at reflux for 3.0 h, was cooled to ambient temperature, and was poured into a solution of 5 mL of 70% perchloric acid in 50 mL of water. The solid was collected by filtration, washed with water and then ether, and recrystallized from methanol containing several drops of perchloric acid. Product yield was 2.27 g (95.8%) of **2b**: ^{1}H NMR (CD_2Cl_2) δ 8.35 (s, 2 H), 8.03 (d, 2 H, J = 9 Hz), 6.95 (d, 2 H, J = 9 Hz), 3.25 (s, 6 H), 1.63 (s, 18 H). Anal. Calcd for $C_{21}H_{30}NSe{\cdot}ClO_4$: C, 53.1; H, 6.4; N, 2.9. Found: C, 53.1; H, 6.4; N, 3.0.

Preparation of 2,6-Di-*tert*-butyl-4-(4-(dimethylamino)-phenyl)thiapyrylium Perchlorate (2c). The procedure described for **2b** was repeated by using 1.12 g (5.0 mmol) of 2,6-di-*tert*-butylthiapyranone. Product yield was 1.92 g (89.6%) of **2c**: ^{1}H NMR (CD_2Cl_2) δ 8.37 (s, 2 H), 8.02 (d, 2 H, J = 9 Hz), 6.91 (d, 2 H, J = 9 Hz), 3.27 (s, 6 H), 1.63 (s, 18 H). Anal. Calcd for $C_{21}H_{30}NS{\cdot}ClO_4$: C, 58.9; H, 7.1; N, 3.3. Found: C, 58.8; H, 7.2; N, 3.2.

Preparation of 2,6-Di-*tert*-butyl-4-(4-(dimethylamino)-phenyl)pyrylium Perchlorate (2d). The procedure described for **2b** was repeated by using 1.04 g (5 mmol) of 2,6-di-*tert*-butylpyranone and substituting fluoroboric acid for perchloric acid. Product yield was 1.80 g (90%) of **2d**: ^{1}H NMR (CD_2Cl_2) δ 8.03 (d, 2 H, J = 9 Hz), 7.57 (s, 2 H), 6.95 (d, 2 H, J = 9 Hz), 3.31 (s, 6 H), 1.53 (s, 18 H). Anal. Calcd for $C_{21}H_{30}NO{\cdot}BF_4$: C, 63.2; H, 7.6; N, 3.5. Found: C, 63.3; H, 7.6; N, 3.6.

Preparation of 2,6-Di-*tert*-butyl-4-methylthiapyrylium Perchlorate (14). To a solution of 1.12 g (5 mmol) of 2,6-di-*tert*-butylthiapyranone in 20 mL of dry THF was added 3.5 mL (10 mmol) of 2.9 M methylmagnesium chloride in THF. The resulting mixture was heated at reflux for 2 h. The solution was cooled and added to dilute perchloric acid. The resulting mixture was allowed to stand 3 h at ambient temperature. The solid was collected, washed with water, and dried under vacuum to give 1.32 g (81%) of **14**, mp 193–194 °C. Anal. Calcd for $C_{14}H_{23}S{\cdot}ClO_4$: C, 52.1; H, 7.2; S, 9.9. Found: C, 51.9; H, 7.3; S, 9.7.

Table XIV. Positional Parameters for Structure 6d[a]

atom	x	y	z	B, Å^2
Te	−0.04633 (2)	−0.04529 (3)	−0.14235 (2)	3.937 (7)
O	−0.2336 (2)	0.4820 (3)	0.0866 (2)	4.03 (7)
CM	−0.0267 (3)	0.2954 (4)	0.0075 (2)	3.6 (1)
C1	−0.1552 (3)	0.0697 (4)	−0.1294 (2)	3.6 (1)
C2	−0.1318 (3)	0.1662 (4)	−0.0868 (2)	3.7 (1)
C3	−0.0355 (3)	0.2036 (4)	−0.0413 (2)	3.39 (9)
C4	0.0571 (3)	0.1517 (4)	−0.0449 (2)	3.6 (1)
C5	0.0725 (3)	0.0541 (4)	−0.0816 (2)	3.5 (1)
C6	−0.1335 (3)	0.5128 (4)	0.1042 (2)	3.4 (1)
C7	−0.0700 (3)	0.4522 (4)	0.0772 (2)	3.5 (1)
C8	−0.1001 (3)	0.3529 (4)	0.0324 (2)	3.4 (1)
C9	−0.2025 (3)	0.3189 (4)	0.0215 (2)	3.8 (1)
C10	−0.2664 (3)	0.3852 (4)	0.0457 (2)	3.8 (1)
C11	−0.1110 (3)	0.6146 (4)	0.1529 (2)	3.6 (1)
C12	−0.0111 (4)	0.6519 (4)	0.1813 (2)	3.9 (1)
C13	0.0109 (4)	0.7472 (5)	0.2275 (3)	4.7 (1)
C14	−0.0658 (4)	0.8056 (5)	0.2460 (3)	4.8 (1)
C15	0.1645 (4)	0.7684 (5)	0.2187 (3)	5.1 (1)
C16	−0.1872 (4)	0.6735 (4)	0.1718 (3)	4.4 (1)
C17	0.1731 (3)	0.0116 (4)	−0.0794 (3)	3.7 (1)
C18	0.2538 (4)	0.0238 (5)	−0.0187 (3)	4.8 (1)
C19	0.3491 (4)	−0.0150 (6)	−0.0183 (4)	6.3 (2)
C20	0.3641 (4)	−0.0657 (6)	−0.0784 (4)	6.4 (2)
C21	0.2863 (4)	−0.0778 (6)	−0.1378 (3)	6.0 (1)
C22	0.1909 (4)	−0.0411 (5)	−0.1392 (3)	4.8 (1)
C23	−0.2596 (4)	0.0398 (5)	−0.1678 (3)	4.2 (1)
C24	−0.2903 (4)	−0.0760 (6)	−0.1780 (3)	5.5 (1)
C25	−0.3900 (5)	−0.1065 (7)	−0.2112 (4)	7.6 (2)
C26	−0.4587 (5)	−0.0189 (8)	−0.2344 (4)	8.3 (2)
C27	−0.4301 (5)	0.0972 (7)	−0.2260 (4)	8.0 (2)
C28	−0.3314 (4)	0.1259 (6)	−0.1925 (3)	6.0 (2)
C29	−0.3738 (3)	0.3627 (4)	0.0329 (3)	4.3 (1)
C30	−0.4225 (4)	0.3928 (5)	0.0827 (3)	5.5 (1)
C31	−0.5238 (4)	0.3685 (6)	0.0703 (4)	6.7 (2)
C32	−0.5756 (4)	0.3124 (6)	0.0084 (4)	6.8 (2)
C33	−0.5289 (4)	0.2815 (6)	−0.0415 (4)	6.4 (2)
C34	−0.4278 (4)	0.3084 (5)	−0.0298 (3)	5.2 (1)
B	−0.2498 (4)	−0.0328 (6)	0.3584 (3)	4.8 (1)
F1	−0.3153 (3)	−0.1065 (4)	0.3146 (2)	9.0 (1)
F2	−0.2997 (4)	0.0672 (4)	0.3651 (3)	11.2 (2)
F3	−0.1711 (3)	−0.0169 (6)	0.3376 (3)	14.5 (2)
F4	−0.2207 (5)	−0.0785 (6)	0.4253 (3)	13.8 (2)
HCM	0.040	0.324	0.027	3.6*
H2	−0.187	0.216	−0.087	3.7*
H4	0.117	0.191	−0.018	3.7*
H7	−0.002	0.477	0.089	3.5*
H9	−0.226	0.248	−0.003	3.8*
H12	0.042	0.612	0.169	3.9*
H13	0.079	0.773	0.246	4.6*
H14	−0.051	0.871	0.277	4.8*
H15	−0.217	0.808	0.232	5.0*
H16	−0.255	0.649	0.153	4.5*
H18	0.244	0.058	0.023	4.7*
H19	0.404	−0.006	0.023	6.2*
H20	0.429	−0.093	−0.078	6.3*
H21	0.297	−0.112	−0.179	6.1*
H22	0.137	−0.051	−0.181	4.8*
H24	−0.242	−0.137	−0.162	5.6*
H25	−0.409	−0.187	−0.218	7.6*
H26	−0.527	−0.039	−0.256	8.5*
H27	−0.478	0.158	−0.244	8.1*
H28	−0.312	0.206	−0.186	6.0*
H30	−0.387	0.432	0.125	5.4*
H31	−0.557	0.390	0.104	6.6*
H32	0.645	0.294	0.000	6.9*
H33	−0.565	0.242	−0.084	6.4*
H34	−0.395	0.289	−0.065	5.2*

[a] Estimated standard deviations are given in parentheses. Parameters with an asterisk were included in the refinement riding on the parent atom. Anisotropically refined atoms are given in the form of the isotropic equivalent displacement parameter defined as $(4/3)[a^2B(1,1) + b^2B(2,2) + c^2B(3,3) + ab(\cos\gamma)B(1,2) + ac(\cos\beta)B(1,3) + bc(\cos\alpha)B(2,3)]$.

Preparation of 2,6-Di-*tert*-butyl-4-methylselenapyrylium Perchlorate (13). The procedure used to prepare **14** was carried out on the same scale with 2,6-di-*tert*-butylselenapyranone. Product yield was 1.63 g (88%) of **13** after recrystallization from ethanol: mp 200–201 °C; ^{1}H NMR (CD_2Cl_2) δ 8.34 (s, 2 H), 2.83 (s, 3 H), 1.66 (s, 18 H). Anal. Calcd for $C_{14}H_{23}S{\cdot}ClO_4$: C, 45.5; H, 6.3; Se, 21.4. Found: C, 45.4; H, 6.2; Se, 21.8.

Preparation of 2,6-Di-*tert*-butyl-4-methylpyrylium Perchlorate (15). The procedure used to prepare **14** was carried out on the same scale with 2,6-di-*tert*-butylpyranone. Product yield was 0.94 g (61%) of **30** following recrystallization from ethanol: mp 203–204 °C; ^{1}H NMR (CD_2Cl_2) δ 7.80 (s, 2 H), 2.81 (s, 3 H), 1.51 (s, 18 H). Anal. Calcd for $C_{14}H_{23}O{\cdot}ClO_4$: C, 54.8; H, 7.6. Found: C, 54.8; H, 7.5.

Preparation of 2,6-Di-*tert*-butyl-4-methyltellurapyrylium Fluoroborate (12). As an alternative to the procedure described in ref 6b for the preparation of **12**, the compound can be prepared by the procedure described for **14**. 2,6-Di-*tert*-butyltellurapyranone (7.00 g, 0.0219 mol) was dissolved in 20 mL of dry THF. Methylmagnesium chloride (20 mL, 2.99 M in THF, 60 mmol) was added dropwise. The resulting mixture was heated at reflux for 2 h and was then cooled to ambient temperature. The reaction mixture was added with stirring to 300 mL of a 10% HBF_4 solution containing 10 g of added sodium fluoroborate. The product was collected by filtration, washed with cold water, and dried under vacuum to give 8.68 g (97%) of **12**: mp 185–187 °C (lit.[6] mp 185–187 °C); ^{1}H NMR (CD_3CN) δ 8.58 (s, 2 H), 2.56 (s, 3 H), 1.55 (s, 18 H).

Preparation of 2,6-Diphenyl-4-ethyltellurapyrylium Hexafluorophosphate (40). 2,6-Diphenyltellurapyranone (1.50 g, 4.17 mmol) was dissolved in 20 mL of dry THF. The resulting solution was cooled to −40 °C, and a 3.1 M in ether solution of ethylmagnesium bromide (7.0 mL, 22 mmol) was added dropwise via syringe. After addition was complete, the reaction mixture was warmed to ambient temperature and was poured into 300 mL of 10% aqueous HPF_6. The resulting precipitate was collected by filtration and was washed with several portions of ether. The precipitate was dissolved in 15 mL of CH_3CN and was filtered through a pad of Celite. The filtrate was diluted with 150 mL of ether. Chilling precipitated a fluffy orange solid that was collected by filtration to give 0.38 g (18%) of **40**, mp 165.5–168 °C. Anal. Calcd for $C_{19}H_{17}Te{\cdot}PF_6$: C, 44.1; H, 3.3. Found: C, 44.3; H, 3.2.

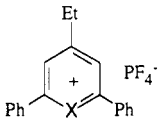

40, X = Te
41, X = Se
42, X = S

Preparation of 2,6-Diphenyl-4-ethylselenapyrylium Hexafluorophosphate (41). 2,6-Diphenylselenapyranone (6.50 g, 0.0209 mmol), 3.1 M ethylmagnesium bromide in ether (22 mL, 0.068 mol), and 300 mL of 10% HPF_6 were treated as described for **40** to give 4.70 g (48%) of **41**, mp 186–189 °C. Anal. Calcd for $C_{19}H_{17}Se{\cdot}PF_6$: C, 48.6; H, 3.7. Found: C, 48.1; H, 3.7.

Preparation of 2,6-Diphenyl-4-ethylthiapyrylium Hexafluorophosphate (42). 2,6-Diphenylthiapyranone (2.76 g, 10.0 mmol), 3.1 M ethylmagnesium bromide in ether (10 mL, 31 mmol), and 150 mL of 10% HPF_6 were treated as described for **40** to give 1.27 g (30%) of **42**, mp 185–187 °C. Anal. Calcd for $C_{19}H_{17}S{\cdot}PF_6$: C, 54.0; H, 4.1. Found: C, 53.9; H, 4.1.

General Procedure for the Preparation of Julolyldyl Dyes 3. The active methyl compounds **12–15** and 1.2 equiv of 9-formyljulolyldine were heated in acetic anhydride (1 mL/mmol) on a steam bath (2 min for **12**, 5 min for **13**, 10 min for **14**, and 20 min for **15**). The reaction mixture was cooled to ambient temperature and diluted with an equal volume of ether. Chilling induced crystallization of the dye. Analytically pure dyes were obtained following recrystallization by dissolving the dyes in CH_3CN followed by dilution of the solution with an equal volume of ether.

For **3a**: 79%; IR (KBr) 2990, 1630, 1510, 1320, 1240, 1205, 1150 cm^{-1}. Anal. Calcd for $C_{27}H_{36}NTe{\cdot}BF_4$: C, 55.1; H, 6.2; N, 2.4; Te, 21.7. Found: C, 55.1; H, 6.2; N, 2.4; Te, 21.2.

For **3b**: 63. Anal. Calcd for $C_{27}H_{36}NSe{\cdot}BF_4$: C, 54.2; H, 6.1; N, 2.3; Se, 13.2. Found: C, 53.8; H, 6.3; N, 2.3; Se, 11.9.

For **3c**: 71%. Anal. Calcd for $C_{27}H_{36}NS{\cdot}BF_4$: C, 65.7; H, 7.4; N, 2.8. Found: C, 65.8; H, 7.3; N, 2.8.

For **3d**: 89%; ^{1}H NMR (CD_2Cl_2) δ 7.90 (d, 1 H, J = 14 Hz), 7.37 (s, 2 H), 7.05 (s, 2 H), 6.82 (d, 1 H, J = 14 Hz), 3.48 (t, 4 H, J = 6 Hz), 2.80 (t, 4 H, J = 6 Hz), 2.01 (quintet, 4 H, J = 6 Hz), 1.42 (s, 18 H). Anal. Calcd for $C_{27}H_{36}NO{\cdot}ClO_4$: C, 66.2; H, 7.4. Found: C, 66.1; H, 7.4.

General Procedure for the Preparation of Monomethine Dyes 4. The active methyl compounds **12–15** and 1.2 equivs of the appropriate 2,6-di-*tert*-butylchalcogenapyranone were heated in acetic anhydride (1 mL/mmol) on a steam bath (2 min for **12**, 5 min for **13**, 10 min for **14**, and 20 min for **15**). The reaction mixture was cooled to ambient temperature and diluted with twice the volume of ether. Chilling precipitated the dyes **4**. Dyes **4a–4d** were prepared by using **12**. Dye **4e** was prepared by using **13**.

For **4a**: 71%; ^{1}H NMR (CD_2Cl_2) δ 7.70 (s, 4 H), 6.72 (s, 1 H), 1.45 (br s, 36 H). Anal. Calcd for $C_{27}H_{41}Te{\cdot}BF_4$: C, 55.9; H, 7.1. Found: C, 56.0; H, 7.2.

For **4b**: 39%; ^{1}H NMR (CD_2Cl_2) δ 7.71 (s, 2 H), 7.67 (s, 2 H), 6.65 (s, 1 H), 1.50 (s, 18 H), 1.49 (s, 18 H). Anal. Calcd for $C_{27}H_{41}SeTe{\cdot}BF_4$: C, 49.2; H, 6.3. Found: C, 49.2; H, 6.5.

For **4c**: 43%; ^{1}H NMR (CD_2Cl_2) δ 7.77 (s, 2 H), 7.65 (s, 2 H), 6.73 (s, 1 H), 1.45 (s, 18 H), 1.33 (s, 18 H). Anal. Calcd for $C_{27}H_{41}STe{\cdot}BF_4$: C, 53.0; H, 6.8. Found: C, 53.3; H, 6.6.

For **4d**: 27%; ^{1}H NMR (CD_2Cl_2) δ 7.75 (s, 2 H), 6.96 (s, 2 H), 6.50 (s, 1 H), 1.45 (s, 18 H), 1.35 (s, 18 H). Anal. Calcd for $C_{27}H_{41}OTe{\cdot}BF_4$: C, 54.4; H, 6.9; Te, 21.4. Found: C, 53.9; H, 6.8; Te, 22.1.

For **4e**: 55%. Anal. Calcd for $C_{27}H_{41}Se_2{\cdot}ClO_4$: C, 52.0; H, 6.6; Se, 25.4. Found: C, 51.8; H, 6.6; Se, 26.1.

For **4f**: 49%. Anal. Calcd for $C_{27}H_{41}SSe{\cdot}ClO_4$: C, 56.3; H, 7.2. Found: C, 56.2; H, 7.2.

For **4g**: 32%. Anal. Calcd for $C_{27}H_{41}OSe{\cdot}ClO_4$: C, 57.9; H, 7.4. Found: C, 57.6; H, 7.3.

Preparation of 4-[(2,6-Diphenyl-4*H*-tellurapyran-4-ylidene)ethyl]-2,6-diphenyltellurapyrylium Hexafluorophosphate (7a). 2,6-Diphenyltellurapyranone (0.28 g, 0.78 mmol) and active ethyl compound **40** (0.35 g, 0.67 mmol) in 2 mL of acetic anhydride were heated on a steam bath for 8 min. The reaction mixture was diluted with 2 mL of CH_2CN and then with 10 mL of ether. Chilling precipitated green crystals of **7a** that were collected by filtration to give 0.32 g (55%) of **7a**. Anal. Calcd for $C_{36}H_{27}Te_2{\cdot}PF_6$: C, 50.3; H, 3.2. Found: C, 50.3; H, 3.2.

Preparation of 7b. 2,6-Diphenyltellurapyranone (0.50 g, 1.4 mmol) and active ethyl compound **41** (0.50 g, 1.1 mmol) in 2 mL of acetic anhydride were heated on a steam bath for 10 min. The reaction mixture was diluted with 5 mL of CH_3CN followed by 40 mL of ether. Chilling precipitated green crystals of **7b** which were collected by filtration to give 0.28 g (33%) of **7b**. Anal. Calcd for $C_{36}H_{27}SeTe{\cdot}PF_6$: C, 53.3; H, 3.4. Found: C, 53.3; H, 3.5.

Preparation of 7c. 2,6-Diphenyltellurapyranone (0.50 g, 1.4 mmol) and active ethyl compound **42** (0.50 g, 1.2 mmol) in 2 mL of acetic anhydride were heated on a steam bath for 20 min. The reaction mixture was diluted with 5 mL of CH_3CN followed by 40 mL of ether. Chilling precipitated green crystals of the dye that were collected by filtration to give 0.62 g (74%) of **7c**. Anal. Calcd for $C_{36}H_{27}STe{\cdot}PF_6$: C, 56.6; H, 3.6. Found: C, 56.3; H, 3.5.

Preparation of 7d. 2,6-Diphenylpyranone (0.030 g 0.12 mmol) and active ethyl compound **40** (0.018 g, 0.035 mmol) in 0.5 mL of acetic anhydride were heated on a steam bath for 10 min. The reaction mixture was diluted with 1.5 mL of CH_3CN followed by 10 mL of ether. Chilling precipitated a bright green solid that was collected by filtration and dried to give 0.012 g (47%) of **7d**. Anal. Calcd for $C_{36}H_{27}OTe{\cdot}PF_6$: C, 57.8; H, 3.6. Found: C, 58.1; H, 3.6.

Preparation of 7e. 2,6-Diphenylselenapyranone (1.50 g, 4.82 mmol) and active ethyl compound **41** (1.96 g, 4.18 mmol) in 5 mL of acetic anhydride were heated on a steam bath for 10 min. The resulting mixture was filtered while hot through Celite. The filtrate was diluted with 50 mL of ether and chilled, precipitating a green, crystalline solid. The solid was collected by filtration and dried to give 2.15 g (67%) of **7e**. Anal. Calcd for

$C_{36}H_{27}Se_2 \cdot PF_6$: C, 56.7; H, 3.6. Found: C, 56.4; H, 3.7.

Preparation of 7f. 2,6-Diphenylthiapyranone (0.052 g, 0.20 mmol) and active ethyl compound **41** (0.047 g, 0.10 mmol) in 0.5 mL of acetic anhydride were heated on a steam bath for 10 min. The reaction mixture was diluted with 1.5 mL of CH_3CN. The resulting solution was diluted with 20 mL of ether and chilled, precipitating a yellow-green solid. The solid was collected by filtration, washed with ether, and dried to give 0.063 g (88%) of **7f**. Anal. Calcd for $C_{36}H_{27}SSe \cdot PF_6$: C, 60.4; H, 3.8. Found: C, 60.0; H, 3.8.

Preparation of 7g. 2,6-Diphenylpyranone (0.050 g, 0.20 mmol) and active ethyl compound **41** in 0.5 mL of acetic anhydride were heated on a steam bath for 10 min. The reaction mixture was chilled for 48 h, precipitating the dye **7g** as chunky, bronze crystals. The crystals were collected by filtration and washed with ether to give 0.043 g (75%) of **7g**. Anal. Calcd for $C_{36}H_{27}OSe \cdot PF_6$: C, 61.8; H, 3.9. Found: C, 61.5; H, 3.9.

Preparation of 4-[(2,6-Diphenyl-4*H*-pyran-4-ylidene)-ethyl]-2,6-diphenylpyrylium Perchlorate (31). A mixture of 5 g of 2,6-diphenylpyranone, 8 mL of propiophenone, and 16 mL of $POCl_3$ was heated on a steam bath for 3 h. The mixture was poured into 50 mL of methanol. Ten mL of 50% perchloric acid was added. The dye precipitated from solution. The dye was collected by filtration and recrystallized from methanol to give **31**, mp 284–285 °C. Anal. Calcd for $C_{36}H_{27}O_2 \cdot ClO_4$: C, 73.2; H, 4.6; Cl, 6.0. Found: C, 73.5; H, 5.0; Cl, 5.9.

Preparation of 9a. Aldehyde **43**[25] (1.0 g, 2.9 mmol) and active methyl compound **12** (1.25 g, 2.9 mmol) in 10 mL of acetic anhydride were heated on a steam bath for 10 min. The reaction mixture was diluted with 100 mL of ether, and the resulting mixture was filtered through Celite. The filtrate was chilled precipitating the dye. The dye was collected by filtration and recrystallized from 3:1 ether–CH_3CN to give 0.70 g (34%) of **9a**: ^1H NMR ($CDCl_3$) δ 8.55 (d, 1 H, J = 13.5 Hz), 7.93 (s, 2 H), 7.57 (s, 2 H), 6.83 (d, 1 H, J = 13.5 Hz), 2.31 (s, 3 H), 1.50 (s, 18 H), 1.45 (s, 18 H). Anal. Calcd for $C_{30}H_{45}Te_2 \cdot BF_4$: C, 48.2; H, 6.1; Te, 34.1. Found: C, 48.0; H, 6.1; Te, 33.1.

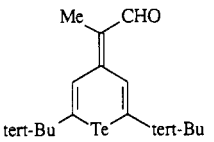

43

Preparation of 9b. Aldehyde **43**[25] (1.55 g, 4.40 mmol) and active methyl compound **13** (1.30 g, 3.5 mmol) in 10 mL of acetic anhydride were heated on a steam bath for 20 min. The reaction mixture was diluted with 150 mL of ether and chilled. Large, chunky, copper–bronze crystals of **9b** were collected by filtration to give 1.01 g (41%) of analytically pure material. ^1H NMR (CD_2Cl_2) δ 8.63 (d, 1 H, J = 13.5 Hz), 7.94 (s, 2 H), 7.57 (s, 2 H), 6.75 (d, 1 H, J = 13.5 Hz), 2.29 (s, 3 H), 1.50 (s, 18 H), 1.48 (s, 18 H). Anal. Calcd for $C_{30}H_{45}SeTe \cdot ClO_4$: C, 50.6; H, 6.4; Te; 17.9. Found: C, 51.0; H, 6.4; Te, 17.3.

Registry No. **2a**, 113160-08-0; **2b**, 113160-10-4; **2c**, 102073-25-6; **2d**, 112135-42-9; **3a**, 104931-03-5; **3b**, 113160-14-8; **3c**, 113160-16-0; **3d**, 113160-18-2; **4a**, 104930-93-0; **4b**, 113160-20-6; **4c**, 113160-22-8; **4d**, 113160-24-0; **4e**, 113160-26-2; **4f**, 113160-28-4; **4g**, 113160-30-8; **5a**, 84790-57-8; **5b**, 54827-49-5; **5c**, 25966-12-5; **5d**, 1537-39-9; **6a**, 83710-79-6; **6b**, 113160-33-1; **6c**, 113160-34-2; **6d**, 83711-01-7; **7a**, 113180-32-8; **7b**, 113160-36-4; **7c**, 113160-38-6; **7d**, 113160-40-0; **7e**, 113160-42-2; **7f**, 113160-44-4; **7g**, 113160-46-6; **8a**, 103817-78-3; **8b**, 104930-95-2; **9a**, 104931-01-3; **9b**, 113160-47-7; **10a**, 83710-87-6; **10b**, 83710-85-4; **10c**, 83710-83-2; **10d**, 83710-81-0; **11**, 113160-69-3; **12**, 103817-93-2; **13**, 113160-58-0; **14**, 71951-56-9; **15**, 2263-20-9; **16**, 113160-60-4; **17**, 289-67-8; **18**, 289-74-7; **19**, 113301-67-0; **20**, 46183-54-4; **21**, 113301-68-1; **22**, 113301-69-2; **23**, 113301-70-5; **24**, 113301-71-6; **25**, 113160-55-7; **26**, 113160-54-6; **27**, 76874-70-9; **28**, 17558-10-0; **29**, 58943-46-7; **30**, 13586-34-0; **31**, 41857-73-2; **36**, 113160-70-6; **37**, 113160-56-8; **38**, 113160-52-4; **39a**$^+$, 51021-41-1; **39b**$^+$, 48232-98-0; **39c**$^+$, 113160-50-2; **39d**$^+$, 113160-51-3; **40**, 113160-62-6; **41**, 113160-64-8; **42**, 113160-65-9; **43**, 113160-66-0.

Supplementary Material Available: Tables of bond distances and angles and crystal data for least-squares planes (5 pages); a listing of structure factors (28 pages). Ordering information is given on any current masthead page.

(25) Wadsworth, D. H.; Detty, M. R.; Murray, B. J.; Weidner, C. H.; Haley, N. F. *J. Org. Chem.* **1984**, *49*, 2676.